

Geotechnical site characterization using surface waves

Kohji Tokimatsu

Tokyo Institute of Technology, Japan

ABSTRACT: Field techniques and analytical procedures for geotechnical site characterization using surface waves are reviewed and summarized in addition to their theoretical background. A modified version of the wavenumber integral approach is introduced for calculating ground surface displacements induced by a point source acting on a three-dimensional layered medium. The effects of body waves and higher-mode Rayleigh waves on the dispersion curves detected by the spectral analysis of surface waves (SASW) method are studied. When a stiff layer overlies a soft layer, body waves and high-mode Rayleigh waves may have significant effects on the observed dispersion curve. The frequency-wavenumber (F-k) spectrum analysis of microtremors method as well as the auto-correlation analysis method is introduced, and phase velocity dispersion characteristics of microtremor ground motions are investigated. It is shown that the F-k analysis of microtremor three-component motions could provide dispersion characteristics of both Rayleigh and Love waves. If a stiff layer overlies a soft layer, a higher-mode or multiple-modes tend to dominate in some frequency range. This makes the dispersion data observed by any of the surface wave methods inversely dispersive. An inversion method capable of considering the effects of higher modes is presented and validated. The S-wave structures estimated from the proposed inversion analysis show good agreement with those obtained by the down-hole method to a depth approximately equal to the maximum sensor distance used. Finally, the applicability and limitation of microtremor H/V spectrum techniques are discussed.

INTRODUCTION

The shear wave profile is the key parameter evaluating dynamic response characteristics of soils. Most of the field tests currently used for determining this property require boreholes, and thus may not be performed conveniently at all cases. Few exceptions are surface-wave methods that enable one to determine S-wave structures without drilling any borehole. Among other surface-based methods such as the reflection and refraction methods, the surface-wave methods appear most promising, considering their potential to detect a relatively soft layer underlying a stiff layer.

The surface-wave methods make use of the dispersive characteristics of surface waves in which their phase velocity varies with wavelength or frequency. The inversion of the dispersion data results in a shear wave profile of the site. This contrasts well with the other geophysical methods that observe P- and S-waves directly. The spectral analysis of surface waves (SASW) method originally introduced by Stokoe and his colleagues into the

geotechnical engineering field has been revised and automated, and is now used for various purposes. Recently, the use of surface waves in microtremors has also been introduced to the geotechnical engineering community for estimating shear structures of sites or for characterizing site effects. The object of this paper is to summarize the state-of-the-arts of the seismic tests using surface waves, with emphasis placed on the use of microtremors.

CLASSIFICATION OF SURFACE WAVE METHODS

The surface wave methods consist of (1) observation of surface waves, (2) determination of their dispersion characteristics, and (3) estimation of shear structure based on inverse analysis of the dispersion curve. Most of the methods currently used observe Rayleigh wave vertical motions. For determining such a dispersion curve, there are essentially two methods, i.e., active and passive methods. Table 1 summarizes the procedures of field observation and

Table 1 Classification of Rayleigh-Wave Methods

Method	Source	Period Range	Array Dimension	Applicable Depth	References
Active	Steady State	less		less than	Jones
	Point Loading	than		10 - 20 m	
	Random Point Loading	about 0.2-0.5 s	Linear		Nazarian and Stokoe
				less than	
Passive	Short-Period Microtremors	less than 1 s	Two-dimensional	50 - 100 m	Tokimatsu et al.
	Long-Period Microtremors	1-5 s		up to several km	Horike, and Okada et al.

in-house analyses, and the period range and applicable depths of these methods.

The active method measures Rayleigh waves in vertical ground vibrations induced either by an impulsive source (Nazarian and Stokoe, 1984; Gabriels et al., 1987; Stokoe et al., 1988; Barker and Stevens, 1991) or an exciter oscillating with a vertical harmonic motion (e.g., Jones, 1958; Tokimatsu et al., 1991). In the active method, sensors are placed on the ground surface in a line with the source, and the phase velocity is computed based on spectrum analysis. The method is suited to explore surface soils to a depth smaller than 10 to 20 meters. Its application to deep soils appears restricted because it is difficult, without a heavy weight, to generate long wavelengths required to determine V_s profiles of deep soils.

The passive method observes either vertical- or three-component motions of microtremors using a two-dimensional array of sensors distributed over the ground surface, without actively generating any vibrations. The wave motion of microtremors is not restricted either to a single mode or to a single direction of propagation (Toksöz, 1964; Asten and Henstridge, 1984). This calls for a large number of sensors to introduce redundancy of information. Based on frequency-wavenumber ($F-k$) spectrum analysis on the vertical motions (e.g., Capon 1969; Lacoss et al. 1969) or spatial auto-correlation analysis (Aki, 1957; Okada and Matsushima, 1986), dispersion characteristics of Rayleigh waves may be determined (e.g., Lacoss et al., 1969; Liaw and McEvilly, 1979; Asten and Henstridge, 1984; Horike, 1985; Okada and Matsushima, 1986). If an extended version of the analysis is applied to the three-component motions, both Rayleigh and Love wave dispersion curves may be obtained (Matsu-

shima and Okada, 1990). The principle in the above method lies in the following facts and assumptions:

(1) Microtremors are considered to be a superposition of traveling surface waves, which constitutes a homogeneous random field.

(2) The vertical motions of microtremors are predominantly Rayleigh waves, while the horizontal motions include Love and Rayleigh waves.

(3) The propagating waves in a stationary random process can be characterized by a frequency-wavenumber power spectral density function or, in some particular cases, by a spatial auto-correlation function. These functions provide the information concerning the phase velocity and percentage power of the propagating waves as a function of frequency.

The method has sometimes been used to characterize deep soil structures, based on the measurements of long-period microtremors in the period range generally longer than 1 s (e.g., Toksöz, 1964; Lacoss et al., 1969; Asten and Henstridge, 1984; Horike 1985; Okada and Matsushima, 1986; Matsushima and Okada, 1990). However, it has seldom been applied to V_s profiling of near-surface soils that requires observation of microtremors in the period range typically shorter than 1 s. This is partly because higher-mode surface waves that tend to dominate in this period range, make both determination and inversion of dispersion curves difficult. In addition, the spectral power of microtremors in a high frequency range is generally low, resulting in a low signal-to-noise ratio. Recently, Tokimatsu et al. (1992b, 1995) have successfully extracted Rayleigh and Love wave dispersion curves from short-period microtremors, and determined shear structures of sites.

CHARACTERISTICS OF SURFACE WAVES

The surface waves are classified into Rayleigh and Love waves, each of which propagates along the surface of a medium. Fig. 1 shows such propagation of Rayleigh waves in which λ is wavelength and D is affected depth. Rayleigh waves consist of vertical and radial horizontal components, and can exist in an elastic half space and a layered half space. Love waves, on the contrary, consist of a transverse horizontal component alone, and can exist only in a layered half space. Most of the surface waves methods currently available observe Rayleigh waves to which the following discussions are limited.

Rayleigh Waves in Homogeneous Elastic Half Space

The wave velocity of Rayleigh waves, V_r , propagat-

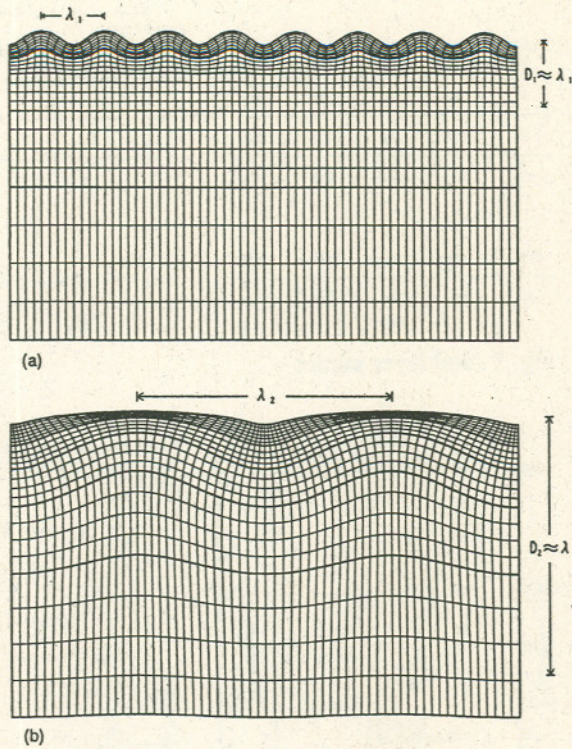


Fig. 1 Propagation of Rayleigh waves with (a) short wavelength and (b) long wavelength

ing along the surface of a homogeneous, isotropic, elastic half space, is independent of frequency or wavelength and is defined by

$$\{2 - (V_r/V_s)^2\}^4 = 16\{1 - (V_r/V_p)^2\}\{1 - V_r/V_s\}^2 \quad (1)$$

in which V_s and V_p are S-wave and P-wave velocities, respectively. Fig 2 shows the relation between V_r/V_s and Poisson's ratio, ν , which is obtained by substituting the following equation into Eq. (1).

$$V_p/V_s = \sqrt{2(1-\nu)/(1-2\nu)} \quad (2)$$

The value of V_r/V_s in Fig. 2 varies from 0.87–0.96 depending on the Poisson's ratio of the half space.

The amplitude ratio between horizontal and vertical motions of Rayleigh waves at the surface of a half space is also independent of frequency and is given by

$$(\dot{u}/\dot{w}) = -2\sqrt{\{1 - (V_r/V_s)^2\}/\{2 - (V_r/V_s)^2\}} \quad (3)$$

in which \dot{u} and \dot{w} are the particle velocities of horizontal and vertical motions, respectively. Since (\dot{u}/\dot{w}) is always an imaginary number with a negative sign, the vertical and horizontal components are out of phase by 90 degrees with each other. Hence,

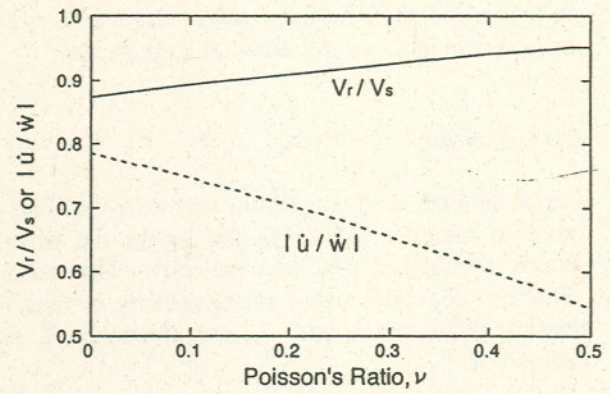


Fig. 2 Effects of Poisson's ratio on V_r/V_s and $|\dot{u}/\dot{w}|$

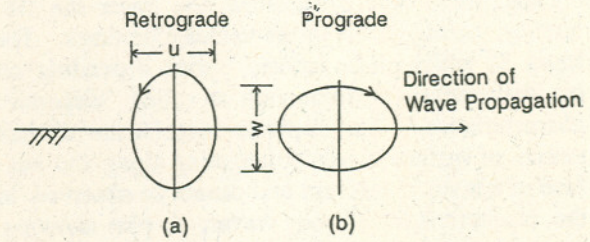


Fig. 3 Particle orbits of Rayleigh waves

the particle motion at a point on the ground during Rayleigh wave propagation is retrograde elliptical (Fig. 3a). The absolute value of (u/\dot{w}) ranges from 0.54–0.79, depending on the Poisson's ratio as shown in Fig. 2.

The particle velocities of Rayleigh waves in either a half or layered medium decay with depth, being negligibly small at depths greater than their propagating wavelengths, as shown in Figs. 1 and 4. The

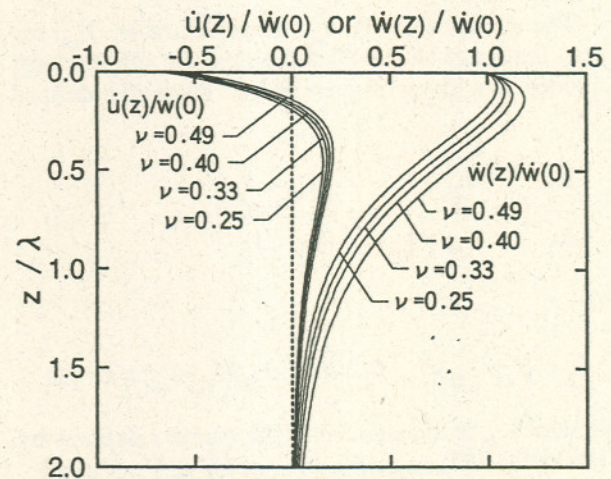


Fig. 4 Mode-shapes of Rayleigh waves in homogeneous elastic half space

waves with short wavelengths thus sample soil properties at small depths, whereas the waves with long wavelengths sample those at large depths.

Dispersive Rayleigh Waves

For a layered elastic medium of which stiffness tends to increase with depth, the longer the wavelength, the higher the wave velocity. The wave velocity, generally called phase velocity, c , has a relation with wavelength, λ , and frequency, f , as defined by

$$c = f \lambda \quad (4)$$

Thus, for a layered medium, the lower the frequency, the higher the phase velocity becomes. The trend in which phase velocity varies depending on the wavelength or frequency is called "dispersive characteristics." The dispersive trend is the distinct nature of surface waves propagating along the surface of a layered medium and cannot be observed in the characteristics of body waves. A plot showing the variation of phase velocity with wavelength or frequency is called "dispersion curve."

Unlike the case of a homogeneous elastic half space, Rayleigh waves in a layered medium show various modes of propagation and each mode propagates at a different phase velocity. These characteristics of Rayleigh waves have been defined, based on the transfer matrix method proposed by Thomson (1950) and Haskell (1953). In their matrix formulation, it is assumed that a layered medium consists of N sublayers as shown in Fig. 5. Each layer is homogeneous and isotropic, and is characterized by thickness, H , mass density, ρ , P-wave velocity, V_p , and S-wave velocity, V_s .

The phase velocity, c_m , or wavenumber, k_m , for the fundamental ($m=0$) and higher ($m>0$) Rayleigh modes at a given frequency, f , is implicitly defined by:

$$\left(\frac{\dot{u}}{w}\right)_m = \frac{J_{22} - J_{12}}{J_{11} - J_{21}} = \frac{J_{42} - J_{32}}{J_{31} - J_{41}} \quad (5)$$

or

$$F_R = (J_{12} - J_{22})(J_{31} - J_{41}) - (J_{11} - J_{21})(J_{32} - J_{42}) = 0 \quad (6)$$

in which J_{ij} is the element of the matrix J defined by Haskell (1953) and a function of H , ρ , V_p , V_s , and c_m or k_m ; and $(\dot{u}/w)_m$ is an imaginary number of m th mode defining the amplitude ratio between the horizontal and vertical particle velocities on the

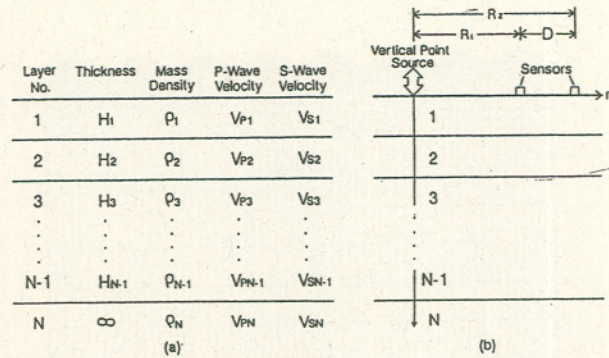


Fig. 5 Soil layer model

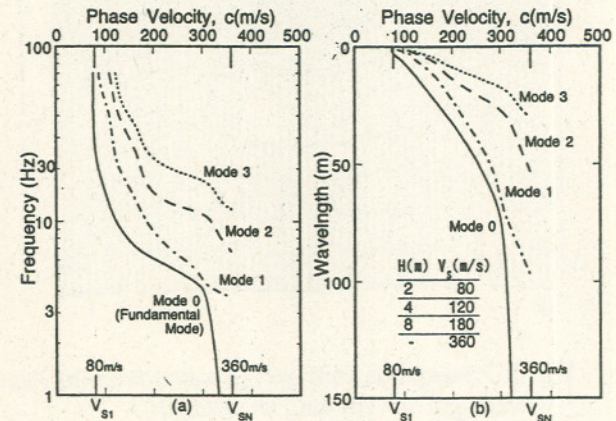


Fig. 6 A typical set of dispersion curves of fundamental and high-mode Rayleigh waves

ground surface. The correlations among c , k , f , and wavelength λ are defined by

$$\lambda_m = \frac{2\pi}{k_m} \quad (7)$$

$$c_m = \frac{2\pi f}{k_m} \quad (8)$$

Fig. 6 shows a set of dispersion curves for a layered medium in which the lowest and highest phase velocities of the fundamental mode are slightly less than the lowest and highest S-wave velocities within the layer. The highest phase velocities of the higher modes are equal to the S-wave velocity of the bottom half space. Fig. 7 shows the mode shapes of the fundamental- and higher-modes at a frequency of 35 Hz. As the order of Rayleigh-mode increases, the corresponding waves reflect soil properties at larger depths, and thus propagate faster.

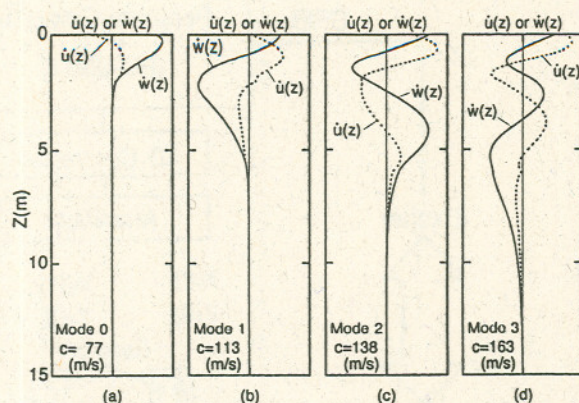


Fig. 7 A typical set of mode-shapes for fundamental and high-mode Rayleigh waves

Horizontal to Vertical Amplitude Ratio of Dispersive Rayleigh Waves

That $(\dot{u}/\dot{w})_m$ in Eq. (5) is an imaginary number means that the vertical particle motion of each mode is either behind or ahead the horizontal one by a phase angle of 90 degrees. This indicates that the particle orbit of each mode is either prograde or retrograde elliptical in the vertical plane containing the direction of propagation of the wave, and that the major and minor axes of the ellipse coincide with the vertical and horizontal axes (Fig. 3).

The actual value of $(\dot{u}/\dot{w})_m$ varies with soil stratification as well as period. For the two-layered-medium ($N=2$ in Fig. 5), such characteristics of the fundamental Rayleigh mode, (\dot{u}/\dot{w}) , were numerically determined, and are shown in Figs. 8 and 9. In Fig. 8, the ordinate is the value of (\dot{u}/\dot{w}) excluding imaginary sign, and the abscissa is the dimensionless period of vertically incident shear waves, T/T_1 , in which $T_1=4H_1/V_{s1}$, and G_2/G_1 is shear modulus ratio of the two-layered medium. In Fig. 9, V_{s2}/V_{s1} is the shear wave velocity ratio. When $\rho_1 = \rho_2$, V_{s2}/V_{s1} corresponds to the impedance ratio between the two layers.

For low shear modulus ratios less than about 4, $(\dot{u}/\dot{w})_0$ is insensitive to dimensionless period, and is always negative. The particle orbit is thus retrograde elliptical, irrespective of period. The trend is similar to that of the half space. As the shear modulus ratio increases, however, the amplitude ratio becomes positive in some dimensionless periods between 1/2 and 1. This means that the particle orbit reverses twice along the period axis if G_2/G_1 exceeds about 5, as shown in Fig. 9. If G_2/G_1 is in between 5 and 8, (\dot{u}/\dot{w}) at the periods of both reversals are zero, i.e., the particle motions are vertical. However, if G_2/G_1 is greater than 8, the particle motion at longer period becomes horizontal.

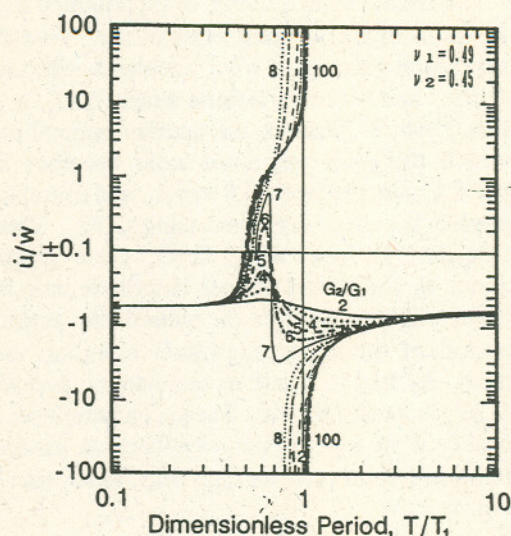


Fig. 8 Variation of Rayleigh wave (\dot{u}/\dot{w}) ratio with dimensionless period for two-layered media having various shear modulus ratios

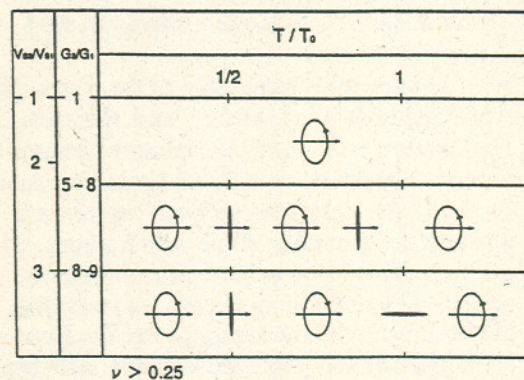


Fig. 9 Variation of Rayleigh wave particle orbit with dimensionless period for two-layered media in terms of shear modulus ratio

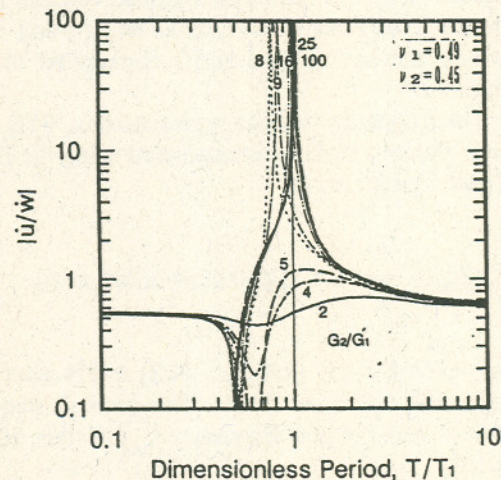


Fig. 10 Variation of Rayleigh wave amplitude ratio with dimensionless period for two-layered media having various shear modulus ratios

This makes (\dot{u}/w) infinite as shown in Fig. 8.

The results shown in Fig. 8 are replotted in Fig. 10 in terms of the absolute value of \dot{u}/w . Note that the maximum value of $|\dot{u}/w|$ increases with increasing G_2/G_1 , and becomes infinite when G_2/G_1 is greater than about 8. Besides, the nondimensional period at which the peak amplitude ratio becomes infinite, takes a value between 0.8 and 1, and asymptotically approaches unity with increasing G_2/G_1 . This means that, for the layer with a G_2/G_1 value greater than about 8, the period of peak amplitude ratio is close to or slightly less than the natural site period. The period of minimum amplitude ratio, on the other hand, is close to a half of the natural period when G_2/G_1 is greater than 8. These characteristics can be observed in any of the two-layered media with Poisson's ratios greater than 0.25, as summarized in Fig. 9.

ACTIVE SURFACE WAVES METHODS

Spectral Analysis of Surface Waves Method

Fig. 11 shows a typical setup of the active Rayleigh wave methods (e.g., Stokoe and Nazarian, 1985). For shallow soil profiling, velocity sensors having natural frequencies of 4.5 or 1 Hz can be successfully used. At least two vertical sensors are placed apart on the ground in a line with a source. A vertical impulsive force or harmonic motions are generated by a hammer or an exciter, and traveling waves are observed with the sensors. The observed records are amplified and digitized with the AD-converter. The AD-conversion and the following spectrum analysis are usually made for a data set of N points at a time interval of Δt . The total duration of the record T is thus $N\Delta t$. The digitized vertical motions in the time domain are defined as $z_1(t)$ and $z_2(t)$ in which the subscripts 1 and 2 correspond to sensor number.

The frequency domain representation, $S_i(f)$, of the time domain motions is expressed using the Discrete Finite Transform as

$$S_{zi}(f_k) = \frac{1}{N} \sum_{n=0}^{N-1} z_i(n\Delta t) \exp[-i(2\pi f_k n\Delta t)] \quad (9)$$

in which $f_k = k/T$ ($k=0,1, \dots, N/2$) and N must be 2^n , e.g., 512, 1024, or 2048. The highest frequency, called the Nyquist frequency f_{\max} , is thus $N/2T$ or $1/2\Delta t$.

The cross power spectrum between the two motions at a frequency f is then given by:

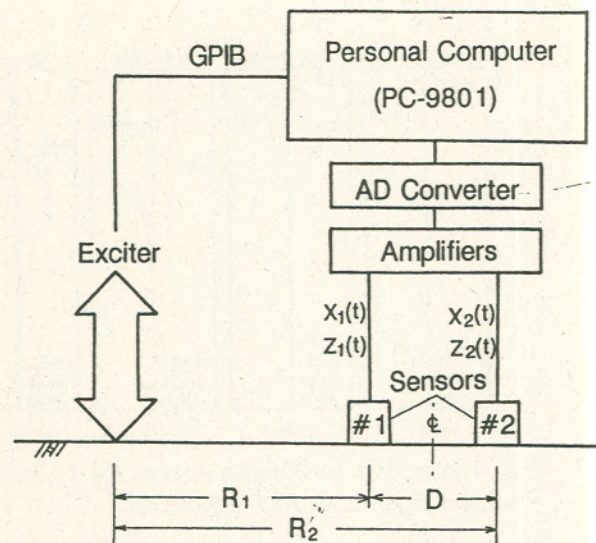


Fig. 11 Typical setup of the active Rayleigh wave methods

$$G_{z_1 z_2}(f) = \frac{1}{M} \sum_{M=1}^M S_{z_1}(f) S_{z_2}^*(f) \quad (10)$$

in which M is the number of digitized data sets, and $*$ indicates the complex conjugate. The quality of the signal may be evaluated with the coherence, $\gamma(f)$, defined as

$$\gamma(f) = G_{z_1 z_2}(f) / [G_{z_1 z_1}(f) G_{z_2 z_2}(f)] \quad (11)$$

Stokoe and Nazarian (1985) suggested that only the signals with high coherence be used for the following phase velocity analysis.

The phase lag of the two motions, ϕ , can be determined by:

$$\phi_v = \tan^{-1} \left[\frac{\text{Im}(G_{z_1 z_2})}{\text{Re}(G_{z_1 z_2})} \right] \quad (12)$$

in which Re and Im indicate the real and imaginary parts of a complex number. The time lag of the two motions, t , is then given by:

$$t = \phi / 2\pi f \quad (13)$$

The phase velocity, c , can be calculated from:

$$c_i = D/t \quad (14)$$

By noting $c = f\lambda$, the corresponding wavelength, λ , can readily be determined.

Nazarian and Desai (1993) reviewed the studies on

the surface wave method (e.g., Sanchez-Salinerio et al., 1987; Sheu et al., 1989), and summarized that the desirable distance between the source and the first sensor is equal to the sensor spacing, and that wavelengths greater than three times the sensor distance should not be considered. This tacitly indicates that the distance from the source and the first receiver should be greater than one third of the maximum wavelength measured.

To satisfy the above requirements, several tests are generally repeated, by expanding the sensor spacing by a factor of 2-3, without changing the imaginary centerline as shown in Fig. 11. Stokoe and Nazarian (1985), and Nazarian and Desai (1993) suggested that after completion of test at each array, the source be moved to the opposite side of the imaginary centerline and testing be repeated. This process cancels the phase shift between sensors, and averages the effects of dipping layers along the observation array, if any (Stokoe and Nazarian, 1985).

If the horizontal motions of traveling waves are measured in addition to the vertical ones, the phase velocity for the horizontal motions can be determined in the same manner as above. This may be useful when the signal-to-noise ratio of the vertical motions is low (Tokimatsu et al., 1991). Besides, the simultaneous measurements of vertical and horizontal motions provide the particle orbit together with its horizontal-to-vertical amplitude ratio, (\dot{u}/\dot{w}) , (see Fig. 3), defined as

$$(\dot{u}/\dot{w})_n = \text{sign}\left\{\tan^{-1}\left(\frac{\text{Im}[G_{xnzn}(f)]}{\text{Re}[G_{xnzn}(f)]}\right)\right\} \frac{S_{xn}(f)}{S_{zn}(f)} \quad (15)$$

in which n indicates sensor number. Although \dot{u}/\dot{w} may be a complex number rather than an imaginary number, the corresponding particle motion can be determined. In the most advanced method, the phase velocities of both vertical and horizontal components, the particle orbit, and the amplitude

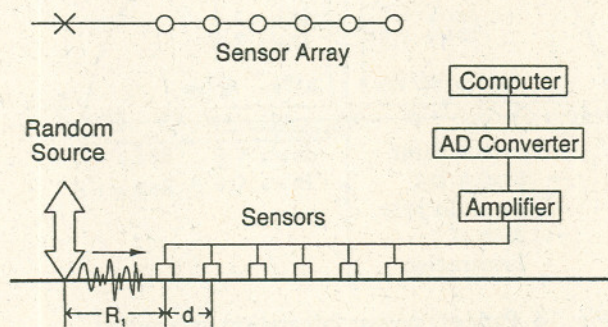


Fig. 12 Typical setup of active Rayleigh wave method with more than two sensors

ratio can readily be shown on the display while the test is in progress (Tokimatsu et al., 1991).

Frequency-Wavenumber Spectral Analysis of Surface waves Method

When the signal-to-noise ratio gets low, the use of more than two vertical sensors with the frequency-wavenumber (F-k) spectrum analysis, e.g., Capon (1969), may work better. Fig. 12 shows a typical test setup with a linear array of six sensors. The F-k spectrum for the array, $P(f,k)$, is defined by

$$P(f,k) = \sum_{i=1}^M \sum_{j=1}^M A_i^*(f,k) A_j(f,k) G_{ij}(f) \exp[ik(x_i - x_j)] \quad (16)$$

where $*$ denotes complex conjugate, f is the frequency, k is the wavenumber in cycles per meter, M = number of sensors, x_j = position of j th sensor, and $G_{ij}(f)$ = cross spectrum between i th and j th sensors given by

$$G_{ij}(f) = \frac{1}{N} \sum_{n=1}^N S_{in}(f) S_{jn}^*(f) \quad (17)$$

in which N is the total number of the nonoverlapping data segments, and S_{in} is the Fourier transform of the data in the i th sensor and in the n th segment; and, for the conventional method, $A_i(f,k) = 1$; or for the high resolution method,

$$A_i(f,k) = \sum_{j=1}^M q_{ij}(f,k) / \sum_{i=1}^M \sum_{j=1}^M q_{ij}(f,k) \quad (18)$$

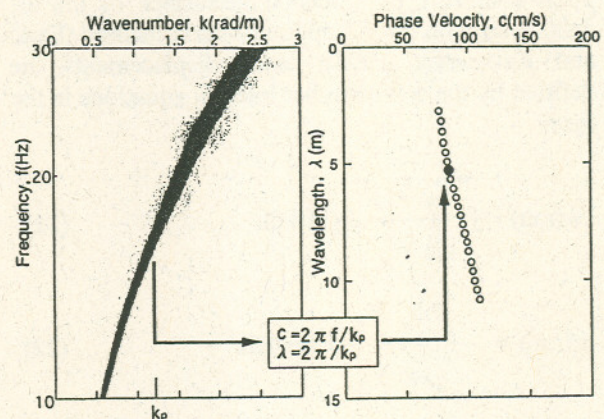


Fig. 13 Typical F-k spectra and corresponding dispersion curve

in which $\{q_{ij}(f, k)\}$ is the inverse of the matrix $\{\exp[ik(x_i - x_j)]G_{ij}(f)\}$. Fig. 13(a) shows a typical example of $F-k$ spectra. By knowing k_p that yields the maximum spectrum power and by substituting its value into Eqs. (7) and (8), a set of phase velocity and wavelength can be determined as shown in Fig. 13(b). The above calculation can readily be done in the field, using a computer equipped with an Intel-486 micro-processor or its equivalent.

To obtain reasonable results, the configuration of the array must satisfy the following (Tokimatsu et al., 1992b):

$$D_{\max} > \lambda_{\max}/3 \quad (19)$$

$$D_{\min} < \lambda_{\min}/2 \quad (20)$$

in which D_{\max} and D_{\min} are the maximum and minimum sensor spaces; and λ_{\max} and λ_{\min} are the maximum and minimum effective wavelengths. Eq. (19) is consistent with the recommendation by Sheu et al. (1989) for the SASW method, and Eq. (20) satisfies the condition for circumventing aliasing in the spectral analysis.

THEORETICAL SOLUTIONS CONCERNING WAVES FROM A POINT SOURCE ACTING ON THE SURFACE OF A LAYERED MEDIUM

Rigorous Solutions Including the Effects of Body Waves

After the pioneer work by Lamb (1904), various methods have been presented for solving the equation of motions in the three-dimensional multi-layered media (e.g., Ewing et al., 1957; Harkrider, 1964; Saito, 1993). Fig. 5 shows such a problem in the cylindrical coordinate where a vertical harmonic point source, $P_0 e^{-i\omega t}$, acts on the surface of the z -axis. Based on the Compound Matrix method (Saito and Kabasawa, 1993), such displacements are defined by the wavenumber integral equations in the form

$$w(r, \omega) = \int_0^\infty \frac{P_0 Y_{14}}{\omega c Y_{24}} J_0(kr) k dk \quad (21)$$

$$u(r, \omega) = - \int_0^\infty \frac{P_0 Y_{12}}{\omega c Y_{24}} J_1(kr) k dk \quad (22)$$

in which $i = \sqrt{-1}$, Y_{12} , Y_{14} , and Y_{24} are variables in the Compound Matrix method, Y_{24} is equivalent to

the characteristic equation defined by Eq. (6); and Y_{14}/Y_{24} and Y_{12}/Y_{24} are given by

$$\frac{Y_{14}}{Y_{24}} = \frac{i[(J_{13}-J_{23})(J_{31}-J_{41})-(J_{11}-J_{21})(J_{33}-J_{43})]c^2}{(J_{12}-J_{22})(J_{31}-J_{41})-(J_{11}-J_{21})(J_{32}-J_{42})} \quad (23)$$

$$\frac{Y_{12}}{Y_{24}} = \frac{[(J_{14}-J_{24})(J_{31}-J_{41})-(J_{11}-J_{21})(J_{34}-J_{44})]c^2}{(J_{12}-J_{22})(J_{31}-J_{41})-(J_{11}-J_{21})(J_{32}-J_{42})} \quad (24)$$

in which J_{ij} is the element of the matrix J defined by Haskell (1953).

A potential difficulty in solving the above integrals is the presence of zero denominator of the integrands. Based on the contour integration in a complex wavenumber plane shown in Fig. 14, Tokimatsu and Tamura (1995) presented a solution of the above in which the displacements of Rayleigh and body waves on the surface are separately determined as

$$\begin{aligned} w(r, \omega) = & - \frac{i}{2} \sum \left[\frac{P_0 Y_{14}}{\omega c (\partial Y_{24} / \partial k)} k H_0^{(1)}(kr) \right]_{k=k_n} \\ & + \frac{i}{2\pi} \int_0^\infty \frac{\omega V_{SN}}{\omega c} \frac{P_0}{Y_{24}} \text{Im} \left(\frac{Y_{14}}{Y_{24}} \right) k H_0^{(1)}(kr) dk \\ & + \frac{1}{\pi^2} \int_0^\infty \frac{P_0}{\omega c} \frac{Y_{14}}{Y_{24}} \text{Re} \left(\frac{Y_{14}}{Y_{24}} \right) k K_0(kr) dk \quad (25) \\ u(r, \omega) = & - \frac{i}{2} \sum \left[\frac{P_0 Y_{12}}{\omega c (\partial Y_{24} / \partial k)} k H_1^{(1)}(kr) \right]_{k=k_n} \end{aligned}$$

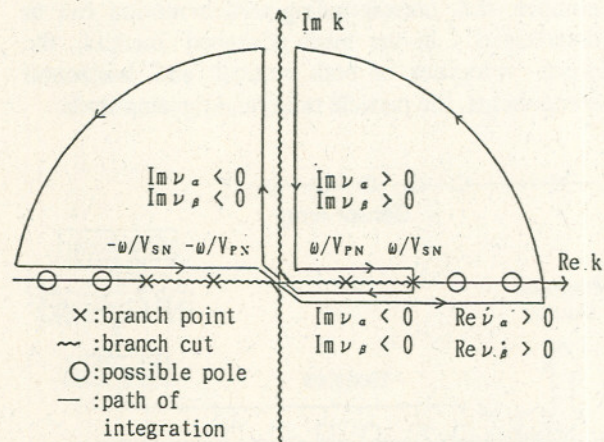


Fig. 14 Path of contour integration in complex wavenumber plane for Eqs. (21) and (22) (after Tokimatsu and Tamura, 1995)

$$\begin{aligned}
& - \frac{i}{2\pi} \int_0^{\infty} \frac{\omega v_{\alpha} P_0}{\omega c} \text{Im} \left(\frac{Y_{12-}}{Y_{24-}} \right) k H_1^{(1)}(kr) dk \\
& - \frac{1}{\pi^2} \int_0^{\infty} \frac{P_0}{\omega c} \text{Im} \left(\frac{Y_{12-}}{Y_{24-}} \right) k K_1(kr) dk \quad (26)
\end{aligned}$$

in which $H_0^{(1)}$ and $H_1^{(1)}$ are Hankel functions of the first kind of order zero and one; K_0 and K_1 are Bessel functions of the second kind of order zero and one; k_m is the wavenumber of the m th mode; Im and Re indicate imaginary and real parts of a complex number; and subscripts + and - indicate that v_{α} and v_{β} defined by the following equations are positive and negative along the path of branch line integration.

$$v_{\alpha}^2 = k^2 - \omega^2/V_{PN}^2 \quad (27)$$

$$v_{\beta}^2 = k^2 - \omega^2/V_{SN}^2 \quad (28)$$

In each of Eqs. (25) and (26), the first term corresponds to the displacement of the residue of Rayleigh poles, and the second and third terms correspond to the contribution of the branch line integrals along the real and imaginary axes, i.e., those of body waves. The ground surface displacements expressed by Eqs. (25) and (26) can be numerically determined, since K_0 and K_1 exponentially decay with increasing wavenumber.

Normal-Mode Solutions for Rayleigh-Waves

When the contribution of body waves is neglected, Eqs. (25) and (26) are reduced to the following equations that are equivalent to those presented by Harkrider (1964):

$$w(r, \omega) = \frac{iP_0}{2} \sum [A_{Rm} H_0^{(1)}(k_m r)] \quad (29)$$

$$u(r, \omega) = \frac{iP_0}{2} \sum [A_{Rm} \left[\frac{\dot{u}}{\dot{w}} \right]_m H_1^{(1)}(k_m r)] \quad (30)$$

in which A_{Rm} is medium response of the m th Rayleigh mode defined by:

$$A_{Rm} = \left[\frac{Y_{14}}{\omega c (\partial Y_{24} / \partial k)} \right]_{k=k_m} \quad (31)$$

and $[\dot{u}/\dot{w}]_m$ is equivalent to Eq. (5) excluding imagi-

nary sign or

$$\left[\frac{\dot{u}}{\dot{w}} \right]_m = - \frac{Y_{12}}{Y_{14}} \quad (32)$$

If $k_m r$ is sufficiently large, say the distance r is more than the wavelength measured, Eqs. (29) and (30) may be approximately given by

$$w_m(r, \omega) \approx \frac{iP_0}{2} \sum A_{Rm} \sqrt{\frac{2}{\pi k_m r}} \exp[i(k_m r - \frac{\pi}{4})] \quad (33)$$

$$u_m(r, \omega) \approx \frac{iP_0}{2} \sum A_{Rm} \sqrt{\frac{2}{\pi k_m r}} \left[\frac{\dot{u}}{\dot{w}} \right]_m \exp[i(k_m r - \frac{3\pi}{4})] \quad (34)$$

The above equations indicate that the relative amplitudes of vertical and horizontal particle motions of each mode for a three dimensional problem can be defined by $A_m/\sqrt{k_m}$ and $A_m/\sqrt{k_m} [\dot{u}/\dot{w}]_m$, respectively. These values are hereby called "response factors" for a three dimensional problem. Similarly, the response factors for a two-dimensional problem are defined as A_m/k_m and $A_m/k_m [\dot{u}/\dot{w}]_m$.

Simulated Dispersion Curves of Rayleigh Waves

Once the distances from the source to the two sensors, R_1 and R_2 , are given, the phase difference between the two can be computed theoretically as

$$\phi_v = \tan^{-1} \left[\frac{\text{Im}(G_{w12})}{\text{Re}(G_{w12})} \right] \quad (35)$$

in which G_{w12} is the cross spectrum defined by

$$G_{w12} = w(R_1, \omega) w^*(R_2, \omega) \quad (36)$$

In the above equation, $w(R_1, \omega)$ and $w(R_2, \omega)$ can be given by either Eq. (25) or (29). The apparent phase velocity for the vertical motion is thus determined by inserting the above result into the following:

$$t = \phi / 2\pi f_k \quad (37)$$

$$c_i = (R_2 - R_1) / t \quad (38)$$

To demonstrate the significance of soil layering on Rayleigh wave propagation, apparent dispersion curves of Rayleigh waves are computed for the three four-layer models listed in Table 2 (Tokimatsu et

Table 2 Soil layer models

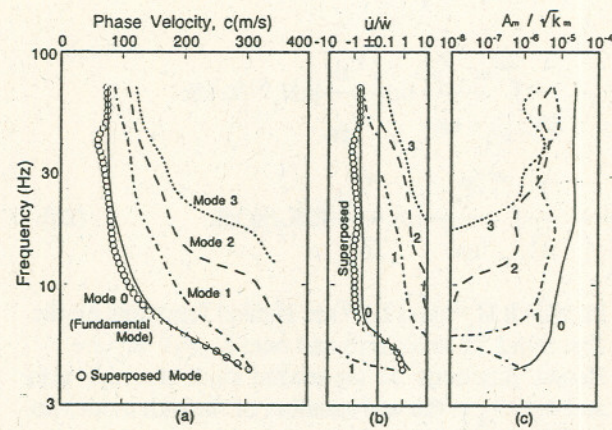
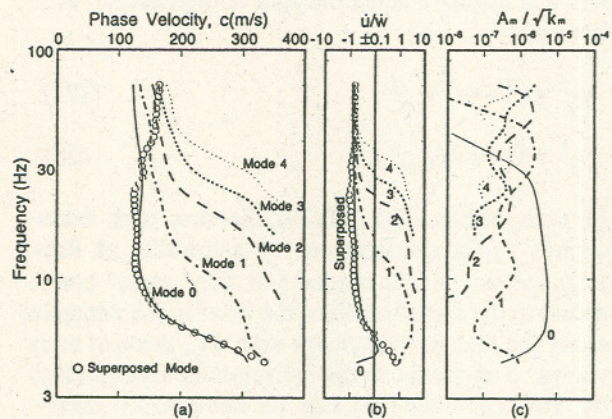
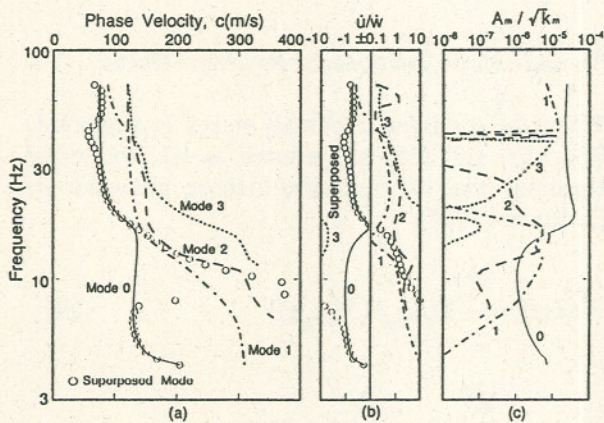
Layer No.	Thickness H (m)	Density ρ (Mg/m ³)	V_p (m/s)	V_s (m/s)		
				Case 1	Case 2	Case 3
(1)	(2)	(3)	(4)	(5)	(6)	(7)
1	2	1.8	360	80	180	80
2	4	1.8	1000	120	120	180
3	8	1.8	1400	180	180	120
4		1.8	1400	360	360	360

al., 1992a). The stiffness of soil layers increases with depth in Case 1, while it varies irregularly with depth in Cases 2 and 3. In the computation, it is assumed that the traveling waves consist solely of Rayleigh waves expressed as Eq. (29) and that these waves are measured with two vertical sensors located at $R_1 = \lambda_0$ and $R_2 = 1.5\lambda_0$ in which λ_0 is the wavelength of the fundamental Rayleigh-mode.

Figs. 15 to 17 summarize the computed results in which the phase velocities, the amplitude ratios, and the response factors of the fundamental and several higher modes are plotted against frequencies. The computed dispersion curves are indicated with the open circles.

In Case 1 with V_s increasing with depth (Fig. 15), the response factors of the fundamental mode are consistently higher than those of any other mode except in the frequency range below 4.5 Hz. The fundamental mode therefore prevails in the vertical and horizontal motions. The dominance of the fundamental mode results in a normally dispersive characteristic for the vertical motion in which the phase velocity increases with decreasing frequency (Gucunski and Woods, 1991).

In Cases 2 and 3, by contrast, a higher mode or multiple higher modes play a significant role in some range of frequency. In Case 2 (Fig. 16), the higher the frequency, the higher becomes the order of higher mode that has the maximum response factor. As a result, higher modes in turn dominate at frequencies over 30 Hz, resulting in an inversely dispersive trend in which the phase velocity decreases with decreasing frequency. A similar trend has been pointed out by Gucunski and Woods (1991). In Case 3 (Fig. 17), either the first or second higher mode has the highest response factor in the frequency range from 9 to 16 Hz, producing an unusual dispersive trend in this range.

Fig. 15 Dispersion curve for Case 1 (after Tokima-tsu et al., 1992a)¹⁾Fig. 16 Dispersion curve for Case 2¹⁾Fig. 17 Dispersion curve for Case 3¹⁾

Effects of Body Waves on Dispersion Curves

For a vertically oscillating source on the surface of a homogeneous, isotropic, elastic half space, Miller and Pursey (1955) showed that two thirds of the total energy goes to Rayleigh waves, while the

remaining goes to body waves. Besides the surface waves attenuate with a square root of distance, whereas the body waves attenuate with a square of distance along the surface (Woods, 1968). Thus, the ground motions enough away from a point source are considered predominant Rayleigh waves. To

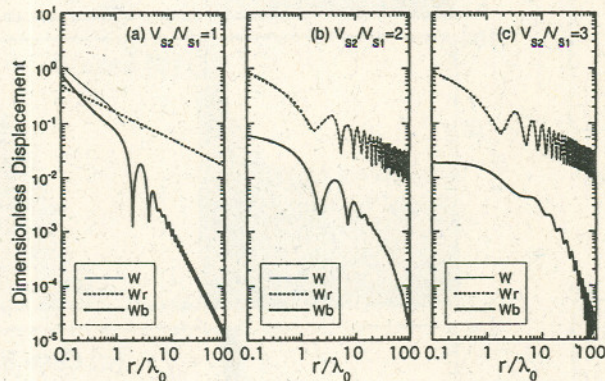


Fig. 18 Dimensionless displacement plotted against dimensionless distance with respect to V_{s2}/V_{s1}

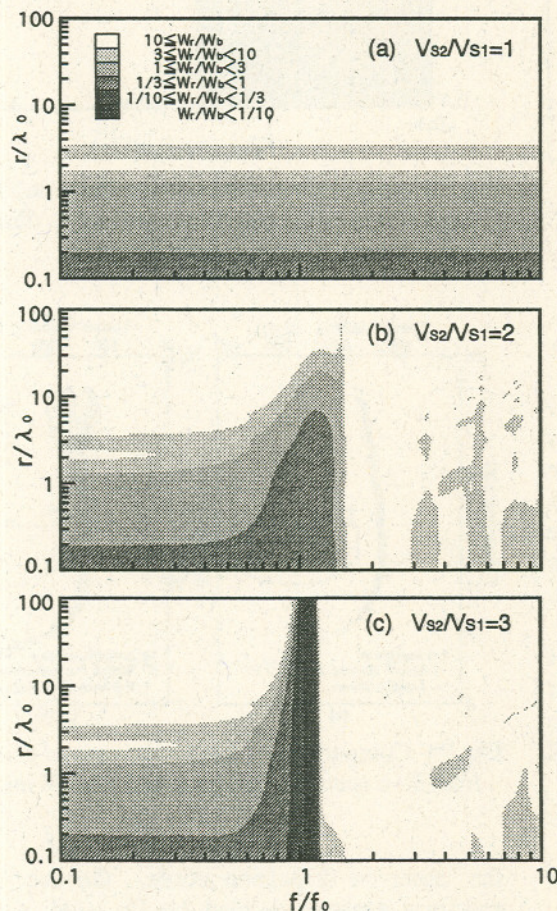


Fig. 19 Amplitude ratios between body and Rayleigh waves with respect to dimensionless frequency, dimensionless distance, and V_{s2}/V_{s1} .

investigate whether the effects of body waves are negligible in a layered medium, the displacements, w , as well as the Rayleigh and body wave components, w_r and w_b , were computed with Eq. (25) for the two-layered media with $V_{s2}/V_{s1} = 1, 2$, and 3.

Fig. 18 shows the dimensionless displacement, $w/[P_o/(\rho V_{s1}^2 H_1)]$, plotted against dimensionless distance at a dimensionless frequency of $f/f_0 = 5$ where $f_0 = V_{s1}/4H_1$. As is the case of a half space (Fig. 18a), most of the energy goes to Rayleigh waves, and Rayleigh waves attenuate in proportion to $r^{-1/2}$, while body waves attenuate in proportion to r^{-2} . Besides, the Rayleigh wave amplitude near the source gets small with increasing V_{s2}/V_{s1} .

Fig. 19 shows the amplitude ratio between body and Rayleigh waves with respect to dimensionless frequency and dimensionless distance. As the value of V_2/V_1 increases, the amplitudes of Rayleigh waves at frequencies higher than the natural frequency become to surpass those of body waves at closer source-to-sensor distance, compared with the case of the homogeneous half space. The frequency range of interest for site characterization using surface waves is inevitably greater than the natural site frequency. It is conceivable therefore that Rayleigh waves generally dominate over the frequency range of interest in the SASW method.

To study whether the effects of body waves in the SASW method are negligible, the dispersion curves of the waves defined by Eqs. (25) and (29), were also computed for the three four-layer models listed in Table 2. Two vertical sensors are set at $R_1 = \alpha\lambda_0$ and $R_2 = R_1 + 0.5\lambda_0$.

Figs. 20 to 22 summarize the computed results in which the phase velocities of all waves from Eq. (25) are compared with those of Rayleigh waves defined by Eq. (29). In Cases 1 and 3 (Figs. 20 and 22), both the dispersion curves are identical with each other, indicating that the effects of body waves

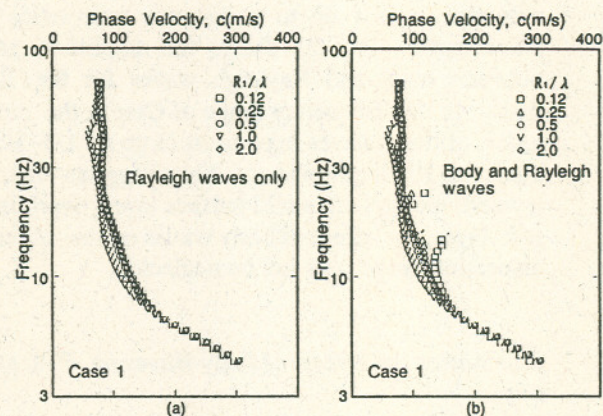


Fig. 20 Effects of body waves on dispersion curves for Case 1

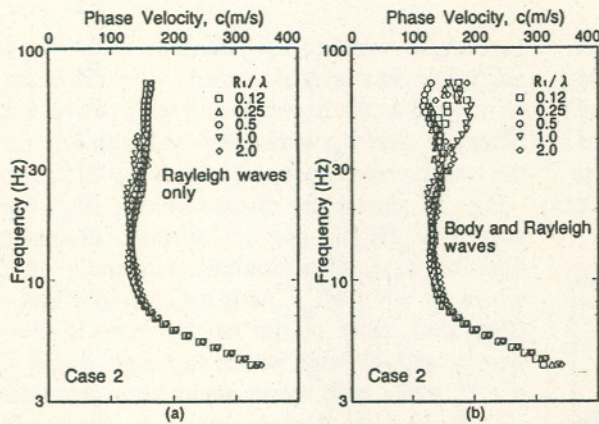


Fig. 21 Effects of body waves on dispersion curves for Case 2

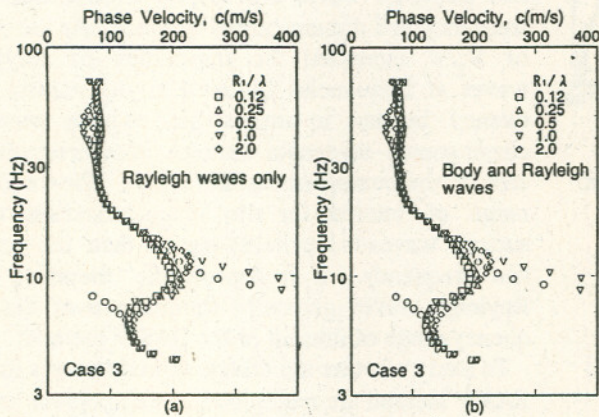


Fig. 22 Effects of body waves on dispersion curves for Case 3

can be neglected if the distance from the source exceeds at least a quarter of the wavelength measured. In Case 2 (Fig. 21), however, the phase velocities of all waves in the frequency range higher than 30 Hz vary significantly and differ from those of Rayleigh waves. Such a variation of phase velocity appears up to a distance over twice the wavelength. Fig. 23 shows the amplitude ratios between body and Rayleigh waves for the three cases. In that frequency range of Case 2, the amplitudes of body waves become as large as 1/3–1/2 of those of Rayleigh waves. This suggests that, for layered media with a stiff surface layer overlying a soft layer, the effect of body waves on the observed dispersion curve may not be neglected.

Elimination of Effects of Body Waves by F-k spectrum

In order to minimize the effects of body waves on

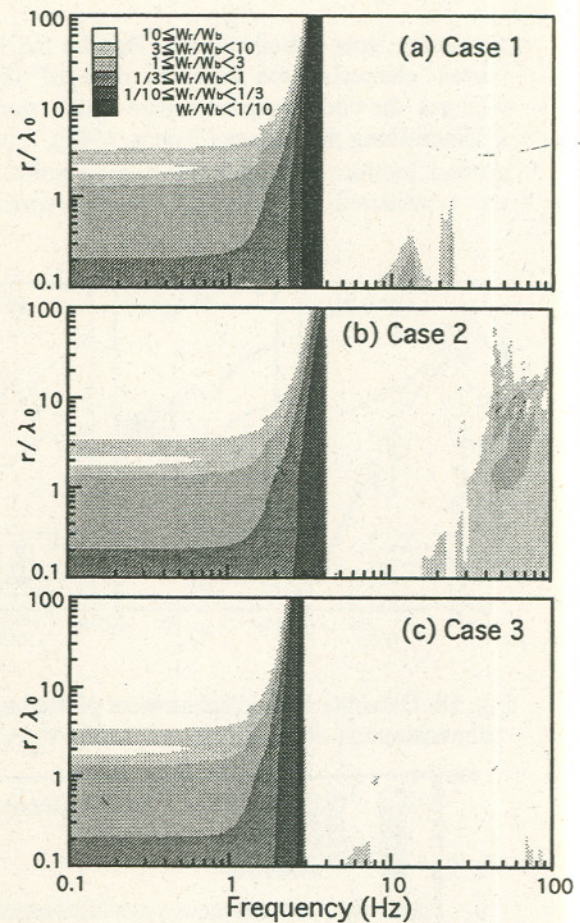


Fig. 23 Amplitude ratios between body and Rayleigh waves with respect to frequency, dimensionless distance, for three cases.

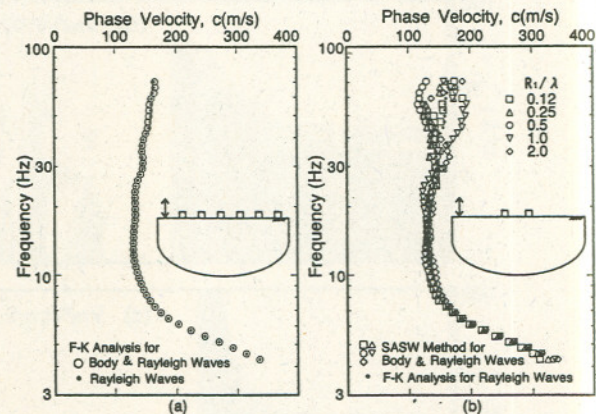


Fig. 24 Comparison of dispersion curves computed from F-k spectrum analysis and SASW method

the observed dispersion curve, the use of F-k spectrum analysis defined by Eq. (16) is studied based on a numerical experiment for Case 2. Six vertical sensors are deployed at equal spaces be-

tween 0.5 and 2.5 times the wavelength from the source. Fig. 24 compares the dispersion curves computed from both the F-k spectrum analysis and the SASW method using two sensors. The F-k spectrum analysis yields a dispersion curve more close to that of Rayleigh waves, suggesting its usefulness to minimize the effects of body waves.

INVERSION PROCESS

Consideration of Higher Modes

A simple method of phase velocity inversion is to assume that the shear wave velocity is approximately equal to about 110 percent of the phase velocity and the effective sampling depth for each wavelength is equal to either 1/3 or 1/2 of that wavelength. Nazarian and Stokoe (1984) indicated that the use of this simple inversion method normally causes some degree of error in the shear wave velocity profiles.

Thus, most of the inversion processes in more advanced methods are based on the theoretical formulation of wave propagation in a layered medium (Thomson, 1950, and Haskell, 1953), assuming that the observed dispersion characteristic is that of the fundamental Rayleigh mode. In reality, however, Rayleigh waves have different modes of propagation and thus different velocities. Besides, the participation of each mode varies depending on soil stratification as well as with frequency. In some cases as described in the preceding chapter, higher modes may be present and could affect overall propagating patterns of Rayleigh waves (Nazarian and Stokoe, 1986; Gucunski and Woods, 1991; Tokimatsu et al., 1992a).

The observed dispersion characteristic in such cases may not necessarily correspond to the fundamental mode but to a higher mode or even multiple modes. The inversion neglecting the effects of higher modes could produce a significant error in the inferred soil profiles. This leads to ambiguity of uniqueness of a soil profile inferred from an inverse analysis if the observed dispersion characteristic is compared with that of the theoretical fundamental mode.

There are two possible cases regarding mode resolution:

(1) A dominant mode and other contributing modes are identified separately, and thus the phase velocities of all of contributing modes can be determined.

(2) A dominant mode and other contributing modes are not resolved separately, and thus only an

apparent phase velocity of the superposed waves of all contributing modes can be determined.

Case 1 calls for a large number of sensors and large array dimensions compared with Case 2. For example, even in the active method using a linear array, 24 sensors deployed over a long distance were used to resolve the fundamental and higher (1 to 6) modes (Gabriels et al., 1987) in the frequency range from 5 to 30 Hz. In contrast, most of the SASW method using a pair of sensors can determine only one dispersion curve and the corresponding mode or modes may not be identified in some cases.

Because of its logistical viability, the method using a limited number of sensors is appealing on the condition that the ambiguity involved in the inverse process is reduced. To reduce such ambiguity, Gucunski and Woods (1991) presented, using so-called stiffness matrix method, the analytical results of the influence of the soil layer properties on the dispersion curve observed with two sensors. Based on the transfer matrix method, Tokimatsu et al. (1992a) also presented a method to calculate simulated dispersion curves for vertical and horizontal motions. A revised version of the method has been described in the previous chapter. The recommendations from these studies include the following:

(1) If the observed data are normally dispersive, the inversion may be made assuming the fundamental mode only, i.e., without considering the effects of higher modes.

(2) If the observed data are inversely dispersive, the effects of multiple modes should be taken into account in the inverse analysis.

(3) Use of either the dispersion data of the horizontal motions or the amplitude ratio of particle motions (Tokimatsu et al., 1991), in addition to the dispersion data of the vertical motions, may reduce the nonuniqueness of the soil profiles resulting from the inverse analysis. Use of both Rayleigh wave phase and group velocities (Baker and Stevens, 1991) or both Rayleigh and Love wave phase velocities may also be possible, if they are successfully determined from the field test.

Inversion Process

If observed phase velocities, c_{ei} , are given at I different frequencies, the goal of the general inversion process is to find a soil layer model that satisfies the following least-squares equation:

$$S = \sum_{i=1}^I (c_{ei} - c_{si})^2 = \text{minimum} \quad (39)$$

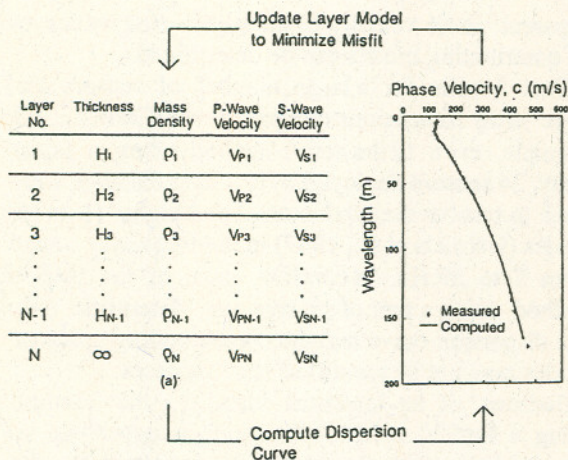


Fig. 25 Diagram showing inversion process

in which c_{si} is the theoretical phase velocity for the fundamental or superposed mode such as given by Eqs. (35)–(38). Eq. (39) may be solved using the nonlinear optimizing method such as proposed by Dorman and Ewing (1962).

The soil layer model is assumed to be horizontally stratified and consists of N layers as shown in Fig. 25. Since the mass density and P-wave velocity have an insignificant effect on the dispersion characteristics, these values are predetermined and only the shear wave velocities or both shear wave velocities and thicknesses are sought. The total number of unknown values, J , is then $2N-1$ or N .

The initial values of the unknown parameters, a_1, a_2, \dots, a_j , are assumed and represented by a column vector, A . The correction vector for A , ΔA , is then evaluated by

$$P \Delta A = C \quad (40)$$

in which P is the matrix with I rows and J columns whose element is $\partial c_{si} / \partial a_j$; C is the column vector whose element is $c_{ci} - c_{si}$.

Various methods for solving Eq. (40) have been described elsewhere (e.g., Dorman and Ewing, 1962; Wiggins, 1972). Once the correction vector is solved, A is updated by $A + \Delta A$. The above computation is repeated until the least mean square, S , becomes almost zero, i. e., the misfit between theoretical and observed dispersion curves is minimized (Fig. 25). The final elements of A are considered to be the actual soil properties to be sought.

Partial Derivative

To solve Eq. (40) requires $I \times J$ partial derivatives of

c_{si} in terms of a_j . These values can be determined numerically by perturbing a_j and computing the change in c_{si} . This is however time consuming since it takes J times the computation time needed for determining one dispersion curve. Instead, the variational technique (Jeffreys, 1961), can be used, in which the partial derivative of phase velocity for a given frequency, c_{si} , with respect to the shear wave velocity of the j th layer, V_{sj} , is given by (Takeuchi and Saito, 1972; and Yuan and Nazarian, 1993)

$$\frac{V_{sj} \partial c_{si}}{c_{si} \partial V_{sj}} = \int_j \frac{1}{\omega^2 I_1} \left(\frac{c_{si}}{U} \right) \left(-y_4^2 + \frac{4kFL}{A - 2L} \dot{y}_1 y_3 \right) dz \quad (41)$$

in which y_1, y_2, y_3 , and y_4 are respectively vertical displacement, normal stress, horizontal displacement, and shear stress, and U_i is group velocity, all can readily be computed for a given frequency, for example, by the transfer matrix method; and $A = \lambda + 2\mu = \rho_j V_{pj}^2$, $L = \mu = \rho_j V_{sj}^2$, $F = \lambda = \rho_j (V_{pj}^2 - 2V_{sj}^2)$, and I_1 is given by

$$I_1 = \int_0^\infty \rho (y_1^2 + y_3^2) dz \quad (42)$$

The determination of partial derivatives in this way only doubles the total computation time for dispersion curves, and thus is recommended to use (e.g., Yuan and Nazarian, 1993).

F-K SPECTRUM ANALYSES OF MICROTREMORS

Array Observation of Microtremors

Figs. 26 and 27 show a typical setup of the array observation of microtremors. In addition to several

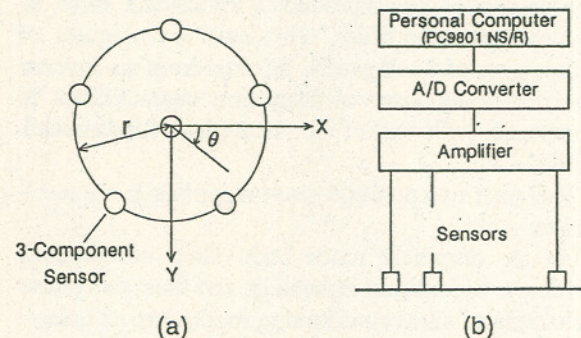


Fig. 26 Schematic diagram for microtremor measurements

vertical or three-component velocity sensors, the test equipment consists of amplifiers, lowpass-filters, 16-bit A/D converter, and a 32-bit computer, all built-in a portable case. The equipment can also be used for the SASW method. Sensors with a natural period of either 1 or 5 s may be used. The computer equipped with the A/D converter can digitize and analyze microtremor data in the field.

Fig. 26(a) illustrates the array used for field observation. In this particular case, five vertical or three-component sensors are placed at equal spacing along the circumference of an imaginary circle drawn on the ground, with one three-component sensor in the center. This means that a total of 8- or 18-component motions is observed simultaneously. The analog motions measured with the sensors are amplified, lowpass-filtered, converted into 2048 or 4096 digitized data each. The sampling rate used varies from 50 to 500 Hz, depending on site geological conditions and array radius used.

Before the microtremor data are stored in the hard-disk of the computer, not only the coherence

between motions but also their phase velocities are computed and displayed as shown in Fig. 28. The spatial auto-correlation analysis described later is suitable for this purpose. It takes less than 10 s with a microcomputer equipped with an Intel 486 processor or equivalent. These analyses enable one to understand the approximate shear structure of the site as well as the signal-to-noise (S/N) ratios of the measured motions, without any delay, thereby enhancing the reliability and performance of the test significantly. The array configuration may not necessarily be circular; however, it is maintained to be circular as much as possible. This is because the spatial auto-correlation analysis can apply only to the data obtained by a circular array. The above procedures are repeated several times until 8 to 16 sets of digitized data are obtained.

The wavelength range that produces reliable phase velocities is given by Eqs. (19) and (20). This means that, for the circular array shown in Fig. 26, the effective wavelength is limited to 2-6 times the array radius used. Therefore, by changing array size, microtremor measurements are repeated, until the phase velocities within the wavelength range of interest are obtained. The test is started, for example, with an array radius of 10 m, and repeated by expanding or contracting the array size by a factor of 2-3. Of course, if more sensors are deployed at different sensor distances, the number of repetition may be reduced. It takes only several to 15 min to complete the observation and the determination of a dispersion curve, if the array radius is less than 50 meters. If the S/N ratios are low, the active method should be used. This situation often occurs in the frequency range over 10-20 Hz and for array radii less than 3 meters, i.e., for waves with short wavelengths.

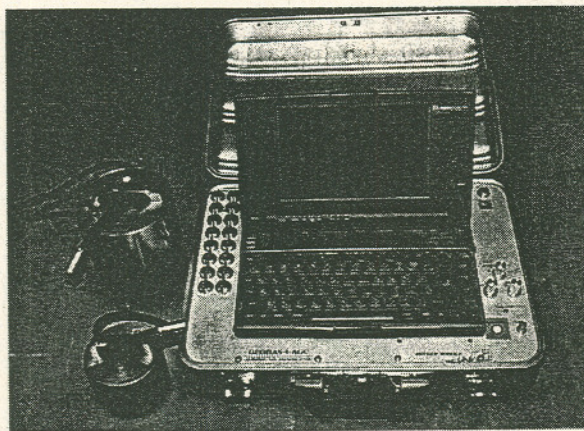


Fig. 27 Instruments for microtremor measurements

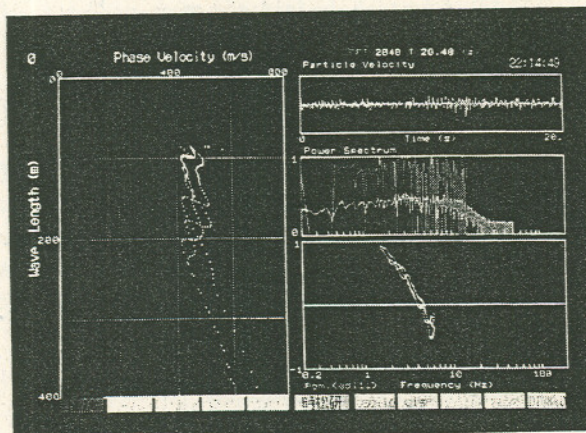


Fig. 28 Computer display showing phase velocity dispersion during test

Vertical Motions

The phase velocity of Rayleigh waves may be determined through the frequency-wavenumber (F-k) spectrum analysis developed by Capon (1969). Assuming that M sensors are available and that the i th sensor is located at the vector position \mathbf{x}_i , the F-k spectrum, $P(f, \mathbf{k})$, is defined by

$$P(f, \mathbf{k}) = \sum_{i=1}^M \sum_{j=1}^M A_i^*(f, \mathbf{k}) A_j(f, \mathbf{k}) G_{ij}(f) \exp[i\mathbf{k} \cdot (\mathbf{x}_i - \mathbf{x}_j)] \quad (43)$$

where $*$ denotes complex conjugate, f is the frequency; \mathbf{k} is the vector wavenumber in cycles per meter defined as

$$k = |k| \exp(i\theta) \quad (44)$$

in which θ is the azimuth of the vector wavenumber, measured clockwise from the x-axis as shown in Fig. 26.

Based on a direct segment method, the cross power spectrum between the i th and j th sensors at a frequency f , $G_{ij}(f)$, is determined by

$$G_{ij}(f) = \frac{1}{N} \sum_{n=1}^N S_{in}(f) S_{jn}^*(f) \quad (45)$$

in which N is the total number of the nonoverlapping data segments, and S_{in} is the Fourier transform of the data in the i th sensor and in the n th segment; and for conventional method $A_i = 1$, and for the high resolution method

$$A_i(f, k) = \sum_{j=1}^M q_{ij}(f, k) / \sum_{i=1}^M \sum_{j=1}^M q_{ij}(f, k) \quad (46)$$

in which $\{q_{ij}(f, k)\}$ is the inverse of the matrix $\{\exp[ik \cdot (x_i - x_j)] G_{ij}(f)\}$.

The F-k spectrum is drawn on a two-dimensional wavenumber ($k_x - k_y$) space for each frequency, as shown in Fig. 29 in which the positive k_y -axis points to the north. The spectra are drawn as contours of $-10 \log[P(f, k)/P_{\max}(f)]$ in which $P_{\max}(f)$ is the maximum value of $P(f, k)$. The maximum of the spectrum power is indicated by an asterisk and the contours of the spectral power are drawn from 0 to 12 dB in steps of 2 dB. The peak of this F-k spectrum provides the information concerning the phase velocity and the azimuth of the source. If a peak occurs at a distance of $|k_p|$ from the origin at a frequency f , the corresponding phase velocity, c ,

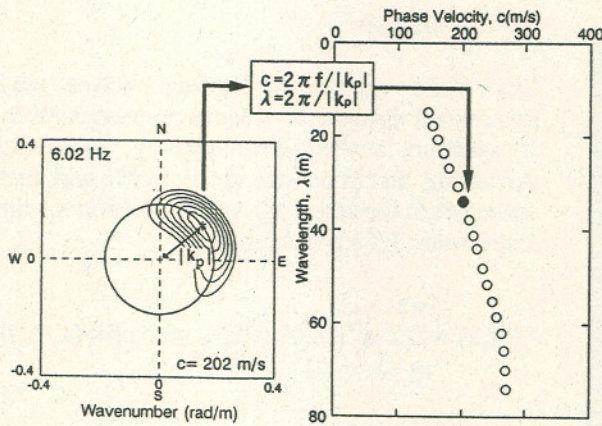


Fig. 29 A typical example of F-k spectra and corresponding dispersion data

and the wavelength, λ , can be given by

$$c = 2\pi f / |k_p| \quad (47)$$

$$\lambda = 2\pi / |k_p| \quad (48)$$

In Fig. 29, for example, $k_p = 0.187$ rad/m, $c = 202$ m/s, $\lambda = 33.6$ m, and the azimuth of the source is the northeast. By repeating the above computation over the frequency range for all data from different array diameters, a dispersion curve can be obtained.

Radial and Transverse Horizontal Motions

Rayleigh waves have a radial horizontal component, and Love waves have a transverse horizontal component. Thus, if microtremors are traveling from one direction and consist mainly of surface waves, their horizontal motions may be decomposed into the radial and transverse components, respectively reflecting Rayleigh and Love waves, by the following (e.g., Haubrich and McCamy, 1969):

$$\begin{Bmatrix} R_i(f) \\ T_i(f) \end{Bmatrix} = \begin{Bmatrix} \cos\theta & \sin\theta \\ -\sin\theta & \cos\theta \end{Bmatrix} \begin{Bmatrix} X_i(f) \\ Y_i(f) \end{Bmatrix} \quad (49)$$

in which θ is the azimuth of the vector wavenumber defined by Eq. (44). The normalized cross spectra for the radial and transverse motions are then defined as (Tokimatsu et al., 1995)

$$G_{r,ij}(f) = R_i(f) R_j^*(f) / (|R_i(f)|^2 |R_j(f)|^2)^{1/2} \quad (50)$$

$$G_{t,ij}(f) = T_i(f) T_j^*(f) / (|T_i(f)|^2 |T_j(f)|^2)^{1/2} \quad (51)$$

in which

$$R_i(f) R_j^*(f) = X_i^*(f) X_j(f) \cos^2\theta + Y_i^*(f) Y_j(f) \sin^2\theta + (X_i^*(f) Y_j(f) + Y_i^*(f) X_j(f)) \sin\theta \cos\theta \quad (52)$$

$$T_i(f) T_j^*(f) = X_i^*(f) X_j(f) \sin^2\theta + Y_i^*(f) Y_j(f) \cos^2\theta - (X_i^*(f) Y_j(f) + Y_i^*(f) X_j(f)) \sin\theta \cos\theta \quad (53)$$

Once replacing G_{ij} in Eq. (43) by either Eq. (50) or (51), the F-k spectra for the radial and transverse motions may be determined. Similar but somewhat different methods have been presented elsewhere (e.g., Haubrich and McCamy, 1969; Horike, 1981).

Combined Horizontal Motions

It is difficult in some cases to decompose horizontal motions into radial and transverse motions, since

these motions are polarized waves (Aki, 1957) to which the application of Eq. (43) is questionable. In those cases, it may be worthwhile to determine the characteristics of combined horizontal motions in which both Rayleigh and Love waves exist. The normalized cross spectrum for the combined horizontal motions is defined as (Tokimatsu et al., 1995)

$$G_{h,jl}(f) = \{X_i^*(f)X_j(f) + Y_i^*(f)Y_j(f)\} / ((|X_i(f)|^2 + |Y_i(f)|^2)^{1/2} (|X_j(f)|^2 + |Y_j(f)|^2)^{1/2}) \quad (54)$$

Unlike Eqs. (50)–(51), the above equation is independent of the azimuth θ , indicating that the combined horizontal motions are unpolarized waves, as is the case for the vertical component. Thus, the F - k spectrum of the combined horizontal motions can readily be determined from Eq. (43), by replacing G_{ij} by Eq. (54). The numerator of Eq. (54) is an arithmetical mean of Eqs. (50) and (51), i.e., the average characteristics of radial and transverse components. Therefore, the phase velocity determined from Eq. (54) would be in between the phase velocities of the radial and transverse components, and their relative position could suggest the ratio of the powers between two components.

SPATIAL AUTO-CORRELATION ANALYSES OF MICROTREMORS

Vertical Motions

If microtremors are measured with a circular array, the phase velocity dispersion can be computed on site with a personal computer, through the spatial auto-correlation analysis, e.g., Aki (1957), Okada and Matsushima (1986), as

$$\rho_v = J_0(rk^R) \quad (55)$$

in which k^R is the wavenumber of the vertical component, i.e., Rayleigh waves, for a frequency f , J_0 is the Bessel function of the first kind of order zero, r is the radius of the array, and ρ_{ave} is the azimuthally averaged auto-correlation coefficient defined by

$$\rho_v = \sum_{i=1}^{M-1} \phi_v(f,i) / \phi_v(f,M) \quad (56)$$

in which $\phi_v(f,i)$ is the spatial auto-correlation function of the vertical motions between the i th sensor and the M th sensor that is located at the center of

the array. By knowing the array radius and the spatial auto-correlation coefficient given by Eq. (56), the wavenumber can be determined from Eq. (55). Substituting this into Eqs. (7) and (8) provides the phase velocity and wavelength.

The phase velocity determined by Eq. (55) is valid only for unidirectional or isotropic waves. However, the on-site computation of dispersion data enables one to understand the outline of the shear structure of the site immediately, thereby enhancing the performance and reliability of the field test significantly.

Transverse Horizontal Motions

Matsushima and Okada (1990) extended the study by Aki (1957), and presented a method to determine the phase velocity of the transverse component, Love waves, c_L , as well as the ratio of the power spectrum densities between the radial and transverse components, i.e., Rayleigh and Love waves, h^R/h^L . If the wavenumber of the radial horizontal motions, k^R , is identical to that of the vertical one determined by Eq. (55) for the same frequency, the unknown values of k^L and h^R/h^L are implicitly determined as

$$\rho_r = \frac{\{J_0(rk^R) - J_2(rk^R)\}h^R + \{J_0(rk^L) + J_2(rk^L)\}h^L}{h^R + h^L} \quad (57)$$

$$\rho_t = \frac{\{J_0(rk^R) + J_2(rk^R)\}h^R + \{J_0(rk^L) - J_2(rk^L)\}h^L}{h^R + h^L} \quad (58)$$

in which J_2 is the Bessel function of the first kind of order two, and ρ_r and ρ_t are defined as

$$\rho_r = \sum_{i=1}^{M-1} \phi_r(f,i) / \phi_r(f,M) \quad (59)$$

$$\rho_t = \sum_{i=1}^{M-1} \phi_t(f,i) / \phi_t(f,M) \quad (60)$$

in which $\phi_r(f,i)$ and $\phi_t(f,i)$ are the spatial auto-correlation function of the radial and transverse horizontal components between the i th and M th sensors.

Again, the phase velocity determined by Eqs. (57) and (58) is valid only for unidirectional or isotropic waves and for the case in which the wavenumbers of vertical and radial horizontal components are equal.

NATURE OF MICROTREMORS

Soil Conditions of Test Sites

To examine whether the F-k spectrum analysis of microtremors can extract the characteristics of surface waves that are independent of source functions, Tokimatsu et al. (1995) conducted field tests at two sites, Yumenoshima and Midorigaoka, hereby called site A and B. At each site, the array observation of microtremors was repeated every 3 hours over a 24-hour period. Site A is located in an artificially reclaimed island in Tokyo Bay. It seems that the major sources of short-period microtremors at the site are traffic on a highway passing from east to west in the south. Site B is in the campus of Tokyo Institute of Technology. The sources of microtremors appear to exist everywhere around the site, as it is surrounded by buildings and streets.

Fig. 30 shows the geological logs at two sites. A relatively thick layer of silt and clay overlies a stiff layer at site A, while a thin soft layer of clay overlies a stiff layer at site B. The natural site periods computed for the shear structures shown in Fig. 1 are 1.39 s for site A and 0.21 s for site B. The array radii used were 7.5, 15, 20, 30, and 48 m at site A, and 3, 5, 10, and 16 m at site B.

Fourier Spectra of Microtremors

Figs. 31 and 32 show the variation of Fourier spectra of the horizontal and vertical motions of microtremors observed every 3 hour over a 24-hour period at sites A and B. Each spectrum was computed by stacking all data components sampled at the corresponding time. The horizontal spectra are

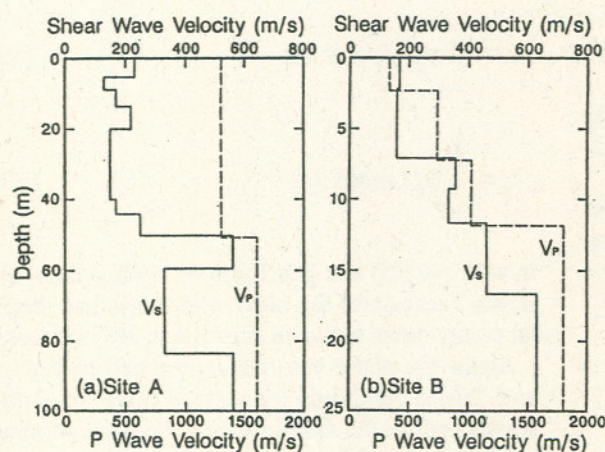


Fig. 30 Geological logs at sites A and B (Tokimatsu et al., 1995)²⁾

defined as

$$S_H = \sqrt{S_{NS} S_{EW}} \quad (61)$$

in which S_{NS} and S_{EW} are the Fourier amplitudes of the two orthogonal horizontal motions.

The spectrum peaks of the horizontal motions occur at periods of 0.35 s at site A (Fig. 31(a)). These peaks may correspond to the theoretical natural site period of the second mode. However, the fundamental natural period at either site cannot be identified from the horizontal spectrum (Figs. 31(a) and 32(a)). The spectra of the vertical motions do not indicate the site periods (Figs. 31(b) and 32(b)), either. Besides, the spectrum at site B is

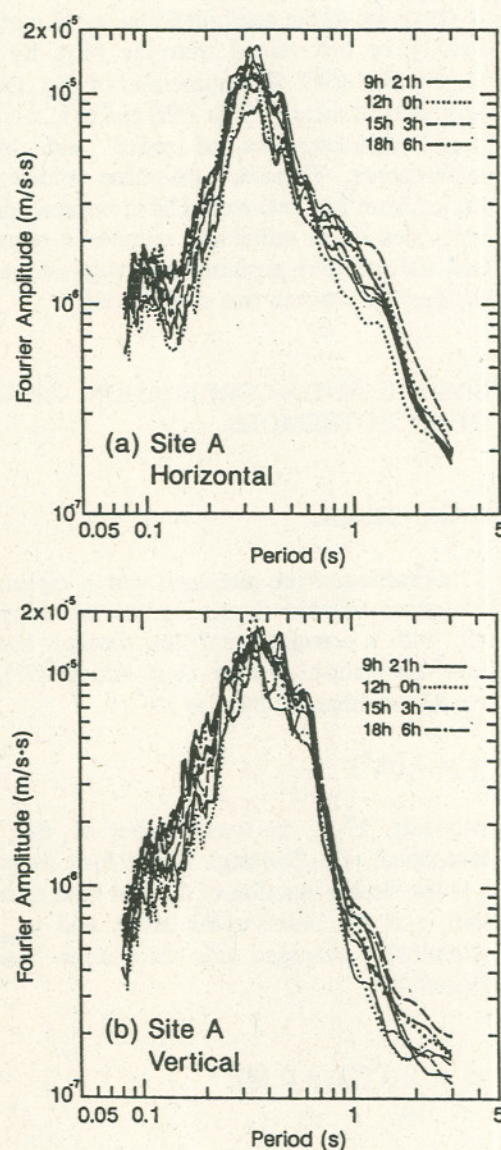


Fig. 31 Fourier spectra of microtremor at site A (a) Horizontal (b) Vertical²⁾

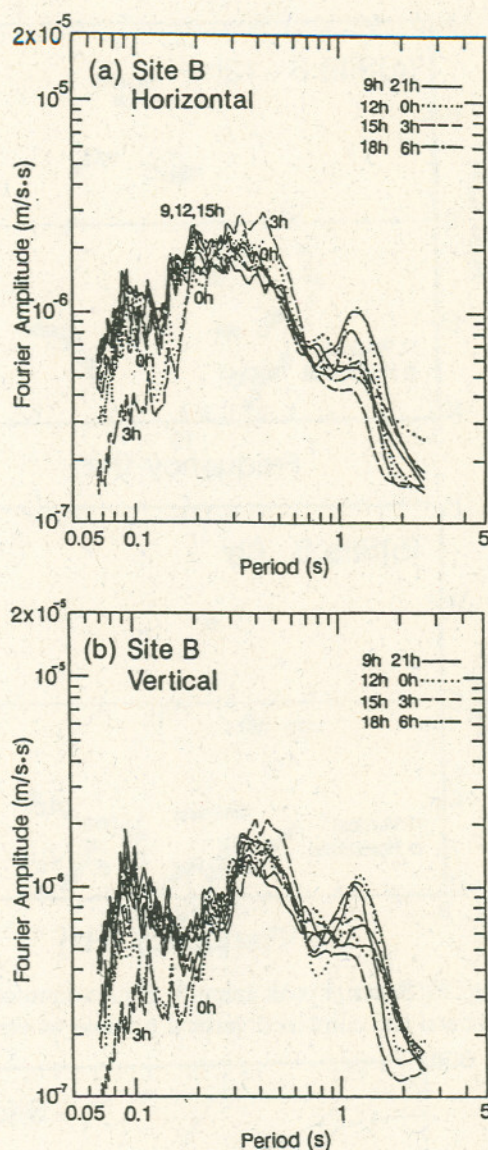


Fig. 32 Fourier spectra of microtremor at site B
(a) Horizontal (b) Vertical²⁾

nonstationary, showing significant decrease during midnight. These findings confirm that the conventional spectrum analysis of microtremors tells more about the exciting function of the source than about the site response characteristics, as indicated by Udwadia and Trifunac (1973).

Dispersion Characteristics of Vertical and Combined Horizontal motions

Figs. 33 and 34 show the high-resolution F-k spectra on a two-dimensional wavenumber space at two frequencies for the vertical and combined horizontal

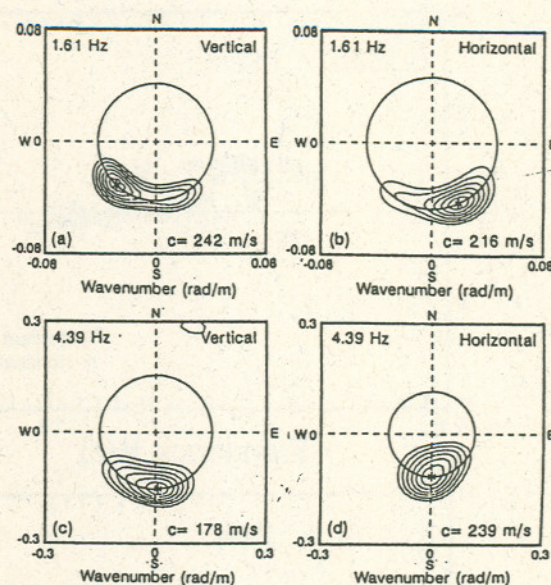


Fig. 33 F-k spectra for vertical and combined horizontal components at site A (12h)²⁾

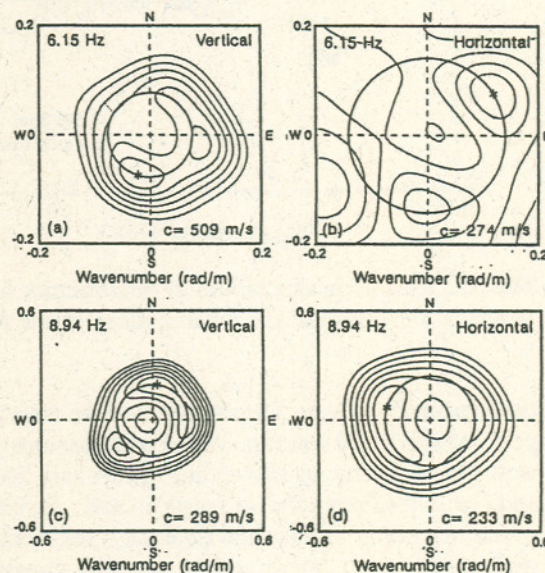


Fig. 34 F-k spectra for vertical and combined horizontal components at site B (12h)²⁾

motions at sites A and B. In each part of Fig. 33, a sharp spectrum peak occurs consistently on the south, indicating that both the vertical and horizontal components at site A propagate mainly from that direction. Fig. 35 shows the variation with frequency of the azimuth of the F-k spectral peak observed during daytime and midnight. The F-k peak azimuth does not change significantly over the frequency range from 1-10 Hz throughout the day (Fig. 35). This suggests that the heavy traffic on the south is the major microtremor source at the site in

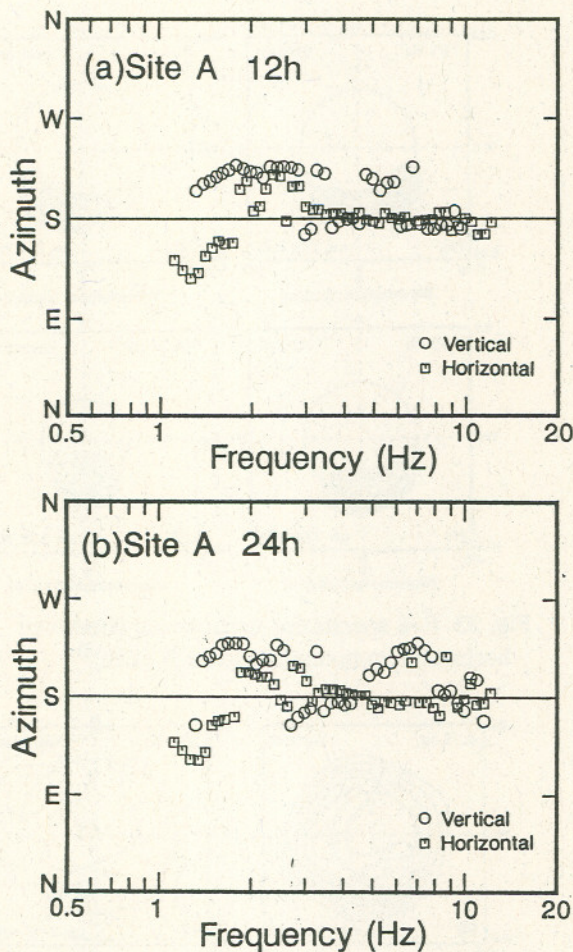


Fig. 35 Spectral peak azimuth of microtremor horizontal and combined vertical motions at site A²⁾

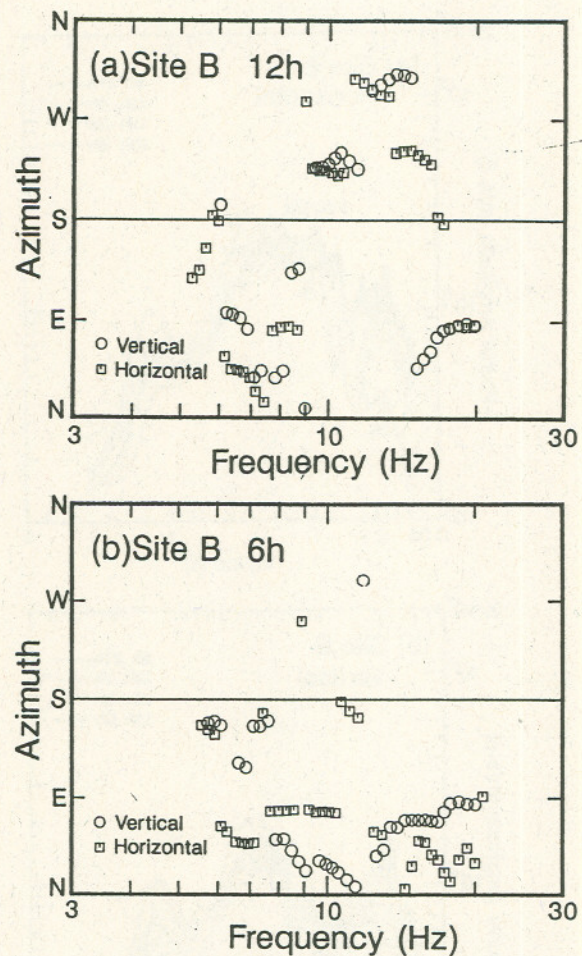


Fig. 36 Spectral peak azimuth of microtremor horizontal and combined vertical motions at site B²⁾

that frequency range. The direction of the spectrum peak at site B, by contrast, varies with frequency as well as with time, as shown in Figs. 34 and 36. In addition, the azimuths of vertical and horizontal spectrum peaks at the same time may not coincide with each other. These trends are also consistent with the microtremor source conditions at the site.

Figs. 37 to 40 summarize the dispersion characteristics from the F-k spectrum analysis for both vertical and horizontal components observed every 3 hours. Despite the non-stationary natures of microtremor spectra shown in Figs. 31 and 32, their dispersion characteristics are stationary over a period of a day at both sites. This means that the F-k analysis of microtremors method could provide site-dependent characteristics in which the effects of exciting function can be eliminated.

Also shown in Figs. 37 and 38 in lines are the theoretical dispersion curves and the response functions up to the 4th higher Rayleigh-mode. The dispersion data show a fairly good agreement with

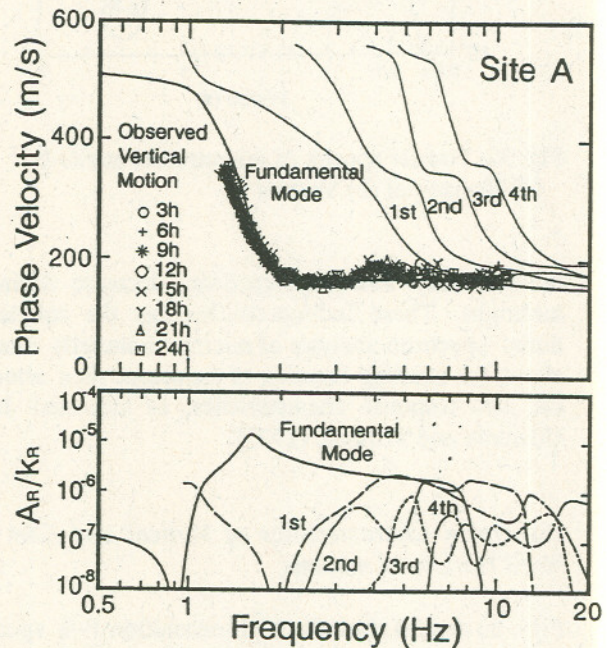


Fig. 37 Dispersion curve from microtremor vertical motions compared with theoretical one at site A²⁾

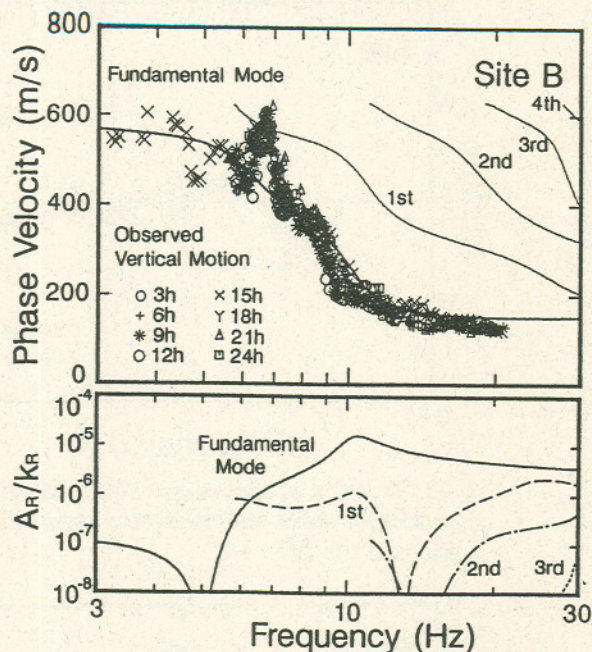


Fig. 38 Dispersion curve from microtremor vertical motions compared with theoretical one at site B²⁾

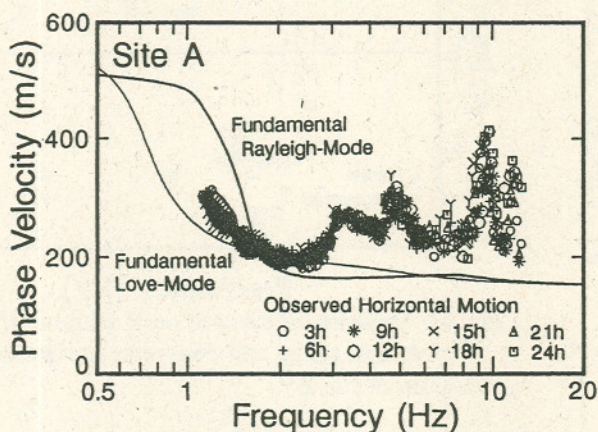


Fig. 39 Dispersion curve from combined horizontal motions compared with theoretical one at site A²⁾

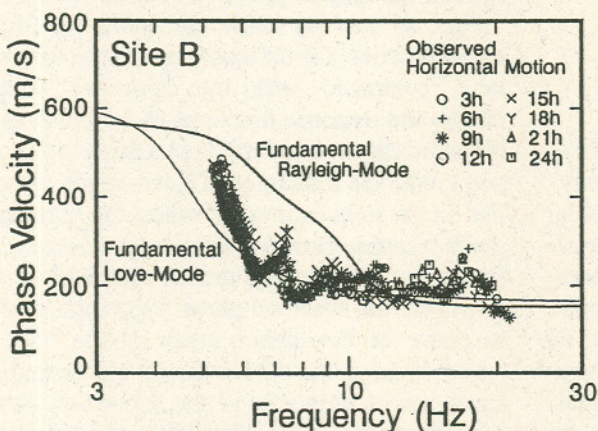


Fig. 40 Dispersion curve from combined horizontal motions compared with theoretical one at site B²⁾

the characteristics of the fundamental Rayleigh-mode in most of the frequency range where the response function of the fundamental mode is the largest among others. In the frequency range from 6–7 Hz at site B, however, the observed phase velocities correspond to those of the 1st higher-mode rather than the fundamental-mode. This is reasonable, when noting that the response function of the 1st higher-mode is comparable with that of the fundamental mode. The relatively good agreement between the observed and computed values suggests that Rayleigh waves dominate in the vertical motions and that the dispersion characteristics extracted from them are those of Rayleigh waves.

Solid lines in Figs. 39 and 40 are the dispersion curves of the fundamental Rayleigh and Love modes, computed for the soil profiles shown in Fig. 30. The observed data for the combined horizontal motions at site A lie in between the two curves at frequencies less than 2 Hz. This suggests that both Rayleigh and Love waves exist in the horizontal motions. The observed phase velocities at site B are close to those of Love waves at frequencies less than 6 Hz, indicating the dominance of Love waves in that frequency range. The observed phase velocities for the combined horizontal motions are higher than any of the two values particularly at site A, showing the presence of higher-modes.

Dispersion Characteristics of Radial and Transverse Horizontal motions

Figs. 41 and 42 show the high-resolution F-k spectra for the radial and transverse horizontal motions at sites A and B, and Figs. 43 and 44 summarize the variation with frequency of their F-k peak azimuths. The azimuths of radial and transverse components at site A coincide with each other, as well as with those of the vertical and combined horizontal components shown in Fig. 35. This confirms that the microtremor source at the site is the traffic on the highway located on the south. The F-k peak azimuths of the radial and transverse components at site B, on the other hand, may not coincide with each other and vary considerably with frequency, indicating that microtremor sources are located at various places around the site.

Figs. 45–46 show the dispersion curves for the radial components. Also shown in the figures in lines are the theoretical dispersion curves and the response functions up to the 3rd–4th higher Rayleigh-modes. The dispersion data at site A show a fairly good agreement with those of the fundamental mode in the frequency range less than 3 Hz where the response functions of the fundamental mode are

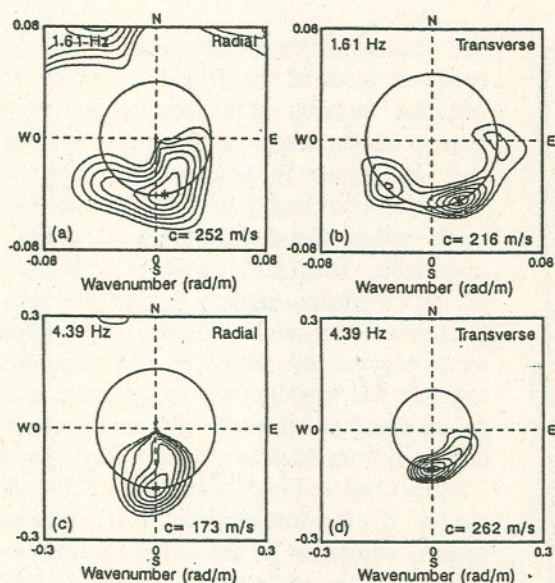


Fig. 41 F-k spectra for radial and transverse horizontal components at site A (12h)²

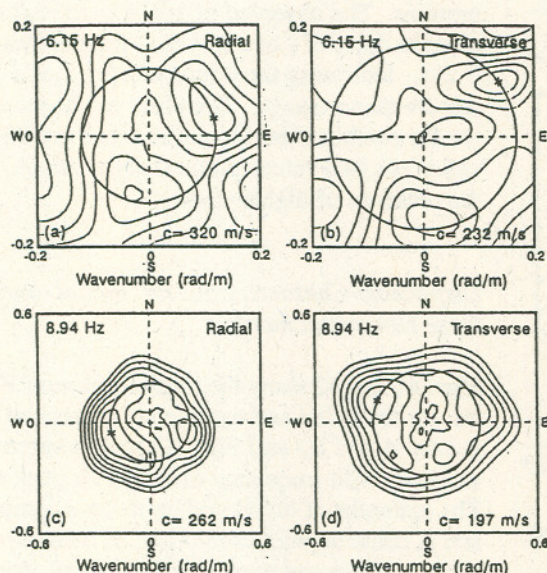


Fig. 42 F-k spectra for radial and transverse horizontal components at site B (12h)²

the largest. The observed phase velocities at frequencies greater than 3 Hz, on the contrary, vary considerably and appear to correspond those of a higher-mode rather than those of the fundamental mode. This is probably because the response functions of the higher modes are comparable with those of the fundamental mode. The dispersion data at site B do not agree with any of the curve shown even in the frequency range where the fundamental mode dominates. It appears therefore difficult to extract Rayleigh wave characteristics from micro-

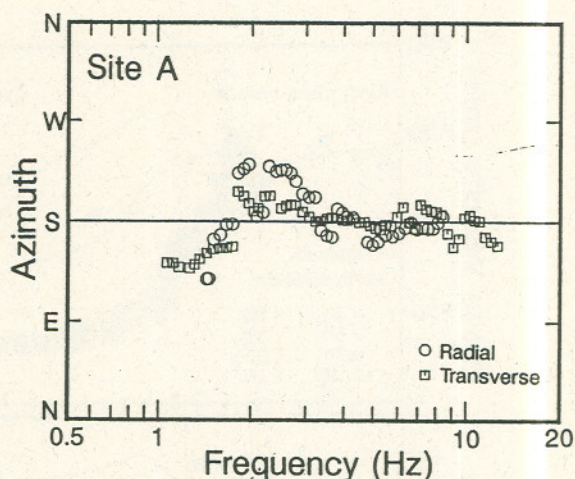


Fig. 43 Variation of spectral peak azimuth of microtremor radial and transverse horizontal motions at site A²

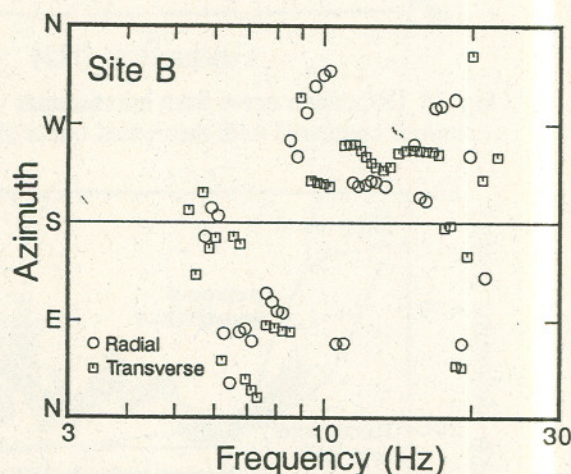


Fig. 44 Variation of spectral peak azimuth of microtremor radial and transverse horizontal motions at site B²

tremor horizontal motions where microtremor sources are located in various places around the site.

Figs. 47 and 48 show the observed dispersion characteristics for the transverse horizontal component, compared with the theoretical dispersion curves and response functions of Love waves. The observed dispersion data show a fairly good agreement with the fundamental Love-mode characteristics in the frequency range where the fundamental-mode response function is the largest among others. In the frequency range greater than 3 Hz at site A, however, the observed phase velocities correspond to those of the higher-mode having the largest response function. It is conceivable therefore that Love waves dominate in the transverse horizontal motions and that the dispersion characteristics extracted from them are those of Love waves.

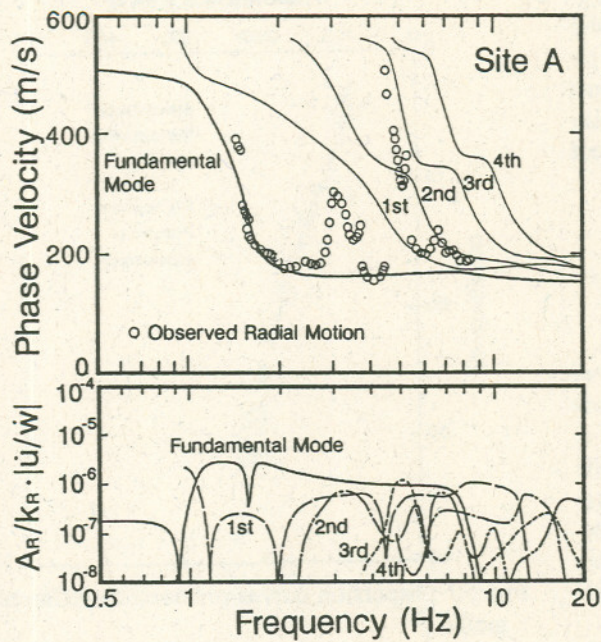


Fig. 45 Dispersion curve from microtremor radial horizontal motions compared with theoretical Rayleigh waves at site A²⁾

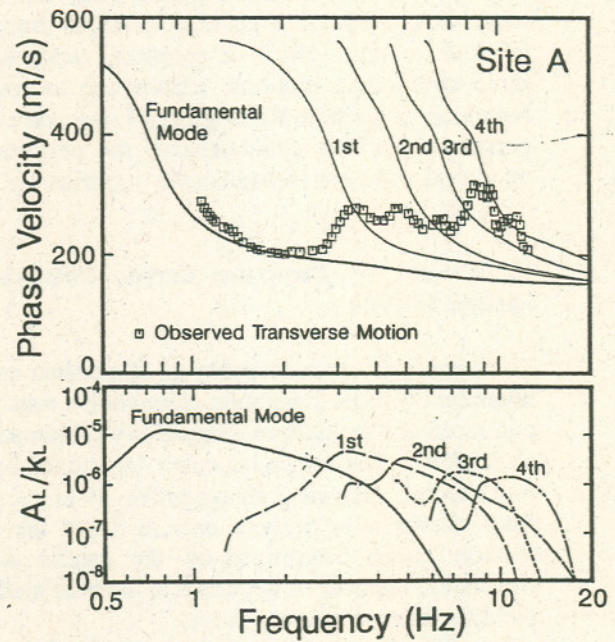


Fig. 47 Dispersion curve from microtremor transverse horizontal motions compared with theoretical Rayleigh waves at site A²⁾

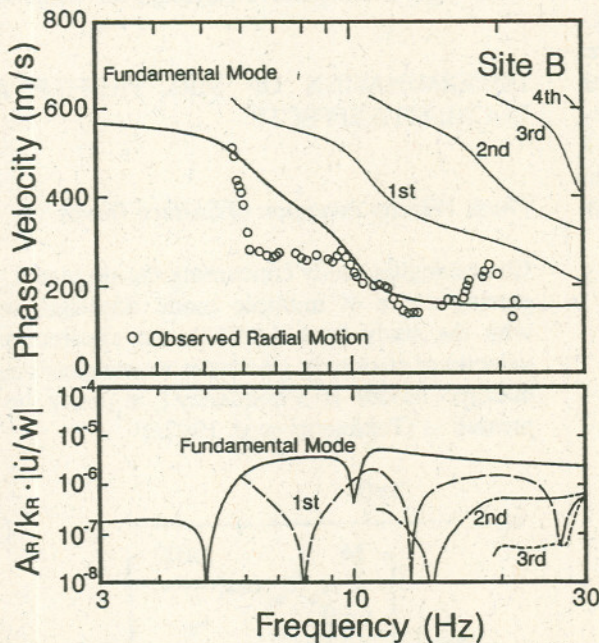


Fig. 46 Dispersion curve from microtremor radial horizontal motions compared with theoretical Rayleigh waves at site B²⁾

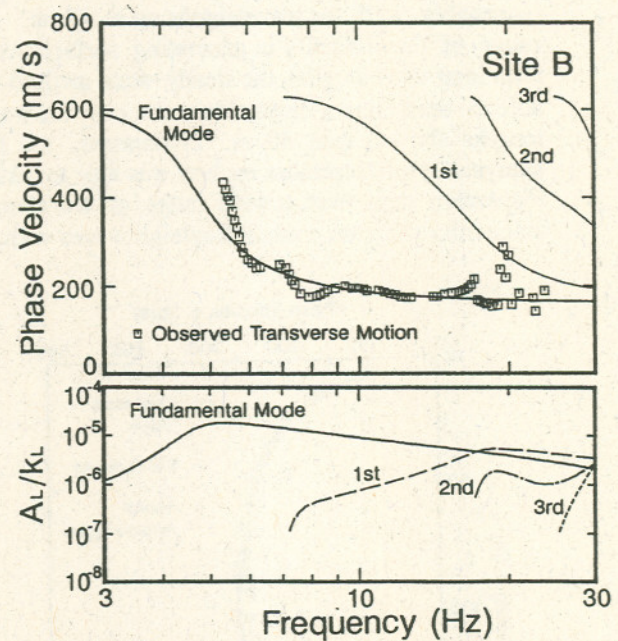


Fig. 48 Dispersion curve from microtremor transverse horizontal motions compared with theoretical Rayleigh waves at site B²⁾

The above analyses and discussions indicate that the microtremor horizontal motions consist mainly of Rayleigh and Love waves. The three-dimensional F-k spectrum analysis presented by Tokimatsu et al. (1995) appears capable of extracting at least one of their dispersion characteristics, i.e., dominate

Love waves, even through microtremors propagate from various directions. If microtremors propagate from one direction, both Rayleigh and Love characteristics may be sampled separately. In addition, the response factor is an efficient indicator to account for the effects of higher modes on microtremor

dispersion characteristics. Considering that Rayleigh wave dispersion can be determined from the vertical motions, the F-k spectrum analysis on three-component motions enables one to conduct inversion using both Rayleigh and Love wave dispersion data. This could enhance the performance on the microtremor measurements significantly.

Comparison of Dispersion Curves Obtained by Various Methods

To investigate the consistency of dispersion curves obtained by various methods, comparative tests were conducted at Kamidokoro, Niigata city (Tokimatsu et al., 1992c). The dispersion curve determined by the F-k spectral analysis is shown in Fig. 49 in crosses. Also shown in the figure in open circles is the dispersion curve determined by the spatial auto-correlation method. It appears that the both methods yield the same dispersion curve.

Fig. 50 compares the dispersion curve obtained from the F-k spectrum method with that from the steady-state Rayleigh wave method. The dispersion curves obtained by the two methods agree reasonably well for wavelengths up to 40 m. Because of the difficulty in generating surface waves with long wavelengths, the steady-state method was able to determine a dispersion curve only for wavelengths shorter than 40 m. In contrast, the F-k analysis of microtremors method was able to extract dispersion data over a wide range of wavelength, since microtremors contain Rayleigh waves with

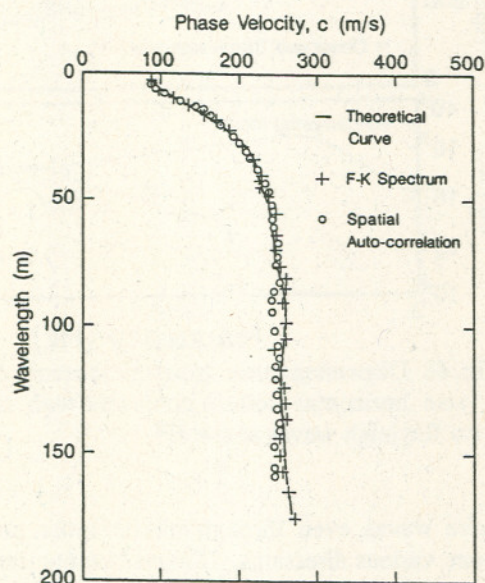


Fig. 49 Observed and computed dispersion curve at Kamidokoro (Tokimatsu et al., 1992c)³⁾

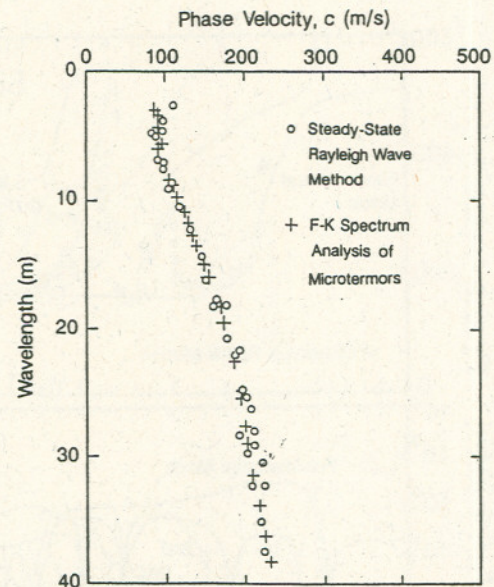


Fig. 50 Dispersion curves obtained by different method³⁾

long wavelengths. This is one of the significant advantages of the passive Rayleigh wave method.

DETERMINATION OF SOIL PROFILE AND LOCAL SITE EFFECTS

Phase Velocity Inversion of Surface Waves

Combining the study concerning the simulated dispersion curve of multiple mode Rayleigh waves, with the study by Aki (1957), the apparent phase velocity of stationary stochastic waves consisting of multiple modes at a frequency f , c_{si} , may be expressed as (Tokimatsu et al. 1992a)

$$c_{si} = \frac{2\pi f D}{\cos^{-1} \left[\frac{\sum_{m=0}^M A_m^2 c_m \cos\left(\frac{2\pi f D}{c_m}\right)}{\sum_{m=0}^M A_m^2 c_m} \right]} \quad (62)$$

in which M is the highest mode considered, D is the distance between sensors, and A_m and c_m are the medium response and the phase velocity of the m th mode of either Rayleigh or Love waves at the given frequency, respectively. Since microtremors are considered to be stationary random waves, their

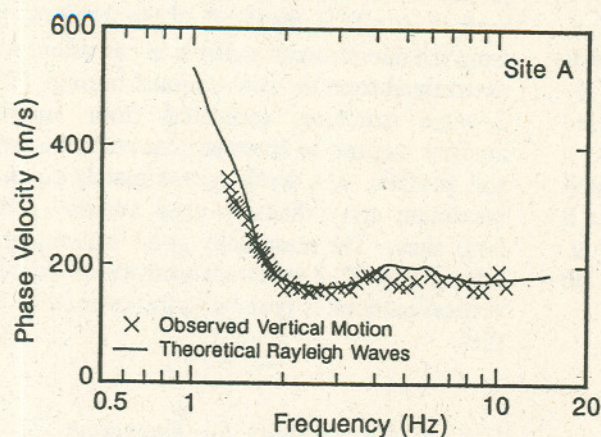


Fig. 51 Dispersion curve of microtremor vertical motions compared with that of theoretical Rayleigh waves at site A

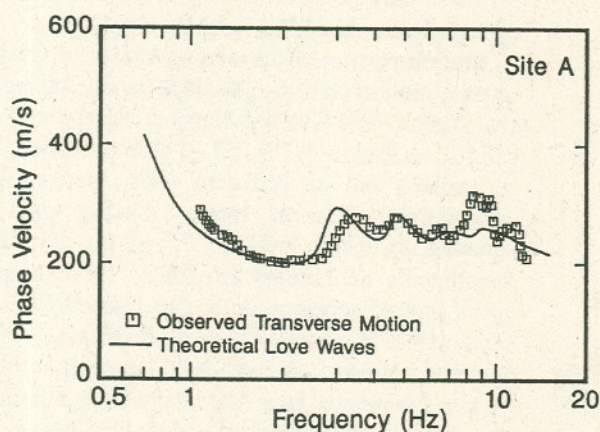


Fig. 52 Dispersion curve of microtremor transverse horizontal motions compared with that of theoretical Love waves at site A

apparent phase velocities may be approximately given by Eq. (62) provided that most of the sources of microtremors are on the ground surface.

The phase velocity dispersion characteristics for sites A and B are computed from Eq. (62) using the geophysical data shown Fig. 30, and compared with the observed ones in Figs. 51 and 52. The computed dispersion curves are in fairly good agreement with the observed ones, indicating that Eq. (62) can be used for determining apparent dispersion characteristics of microtremors.

Shear Wave Velocity Profiles Obtained by Inversion of Microtremor Dispersion Curve

Tokimatsu et al. (1992b) compared the shear wave velocity profiles from the F-k spectrum analysis of

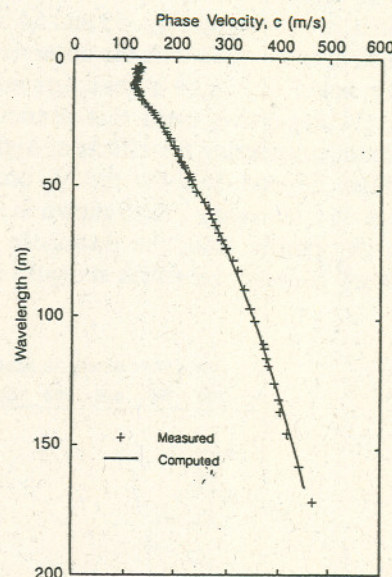


Fig. 53 Observed and computed dispersion curves at Makuhari (after Tokimatsu et al., 1992b)⁴⁾

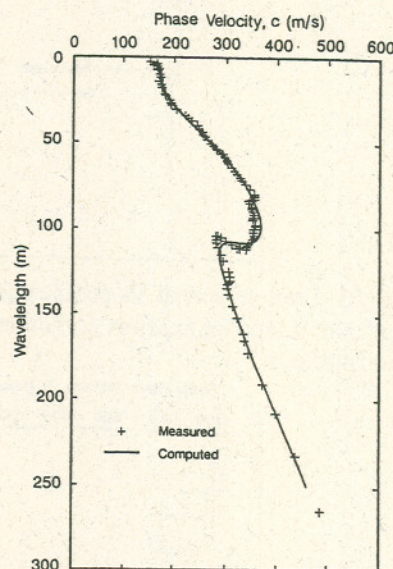


Fig. 54 Observed and computed dispersion curves at Marina⁴⁾

microtremor vertical motions with those obtained by the downhole method. Figs. 53 and 54 show the dispersion curves at Makuhari and Marina sites. The maximum array radii used are about 30 meters at both sites. The observed data at Makuhari site show a normally dispersive trend; however, those at Marina site show an inversely dispersive trend, suggesting the presence of a higher or multiple Rayleigh modes. It appears that the primary factor for this tendency is the presence of the stiff layer between 11.6 and 22.9 meters that overlies a softer layer.

The dispersion curves for the inverted soil layer model are shown in Figs. 53 and 54 in a solid line, which is compatible with the observed data. Particularly noted in Fig. 54 is good agreement in the inversely dispersive trend that cannot be simulated without considering the effects of higher modes.

Figs. 55 and 56 show the V_s profile estimated from the inversion. Also shown in each figure is the V_s profile from the downhole method. Although S-wave velocities at depths larger than 30

meters were not determined by the downhole method at site B, the depth of the bedrock inferred from the microtremor analysis is consistent with that determined from the conventional boring. Thus, the S-wave structures estimated from microtremor analysis appear to be consistent with the available soil profiles, to a depth approximately equal to the maximum array diameter used, i.e., 60–80 m for both sites. The reasonably good agreement indicates that the F–k spectrum analysis of microtremor vertical motions is promising for estimating V_s profiles.

Use of Microtremors for Estimating Local Site Conditions

Tokimatsu and Arai (1995) studied possible use of short-period microtremors for estimating local site effects. Described following is the brief results of the study conducted in Kushiro city, Japan.

Microtremor measurements were conducted at two strong motion stations (Kushiro Japan Meteorological Agency and Kushiro Harbor), hereby call sites J and H, as shown in Fig. 57. These two sites, located nearby but on different soils, were shaken in a completely different manner during past earthquakes, as listed in Table 3. In the Kushiro-oki earthquake of January 15, 1993, for example, the peak ground acceleration at site J was 0.73 G, while that at site H was 0.48 G (e.g., Kashima, 1993; and Iai et al., 1994). In any case, the peak acceleration at site J is greater than that at site H by a factor of 2–4. Site H is situated on a deep Holocene deposit that overlies Tertiary Rock at a depth more than 77 m. Site J, on the other hand, is located on a hill covered by a thin volcanic deposit that is underlain

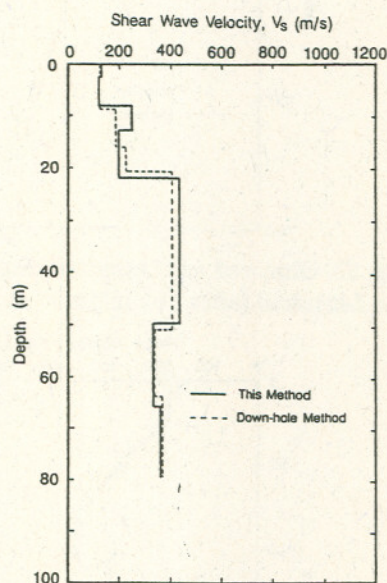


Fig. 55 Comparison of V_s profiles determined from microtremor F–k analysis and down-hole method at Makuhari⁴⁾

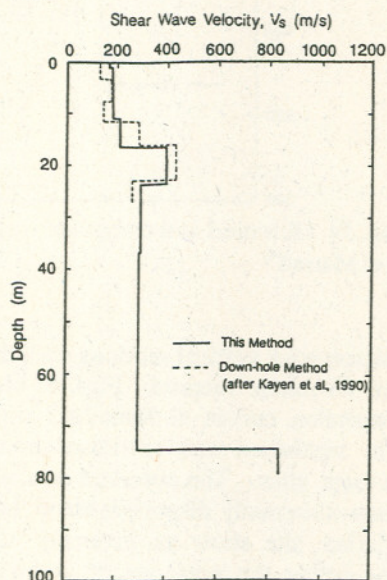


Fig. 56 Comparison of V_s profiles determined from microtremor F–k analysis and down-hole method at Marina⁴⁾

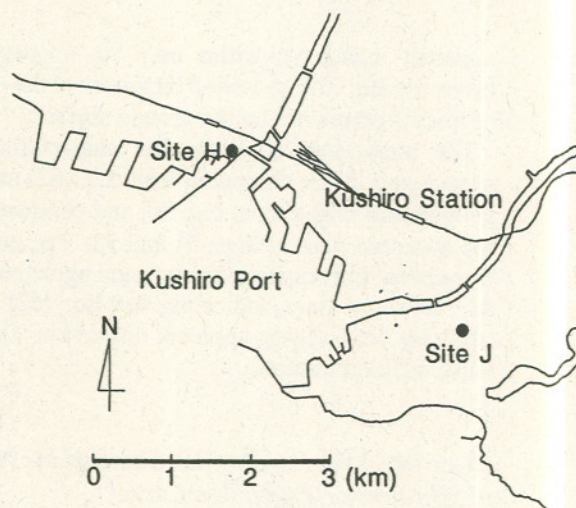


Fig. 57 Map showing observation sites (after Tokimatsu and Arai, 1995)⁵⁾

Table 3 Peak ground accelerations at Kushiro
JMA and Kushiro Harbor (in cm/s^2)

	Kushiro JMA		Kushiro Harbor	
	N63E	N153E	NS	EW
10/10/88	174.4	168.1	45.4*	60.0*
1/15/93	711.4	637.2	469.3	344.2
2/04/93	53.6	74.2	16.4	18.3

* uncorrected

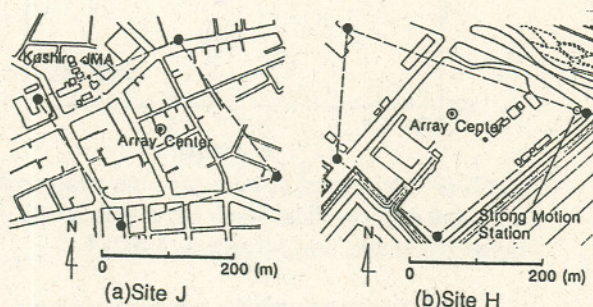


Fig. 58 Maximum aperture array used at sites J and H⁵⁾

by Tertiary Rock. The minimum and maximum sensor spacings were 3 and 160 m at site J, and 3 and 200 m at site H. Figs. 58(a) and (b) show the array centers and the maximum aperture arrays used at the sites.

The dispersion data resulting from the F-k spectrum analysis of the microtremor records are shown in Figs. 59(a) and 60(a) in open circles. The data appear to show normally dispersive trends, except for a small wavelength range. Fig. 59(b) shows the V_s profile estimated from the inversion. The theoretical dispersion curves for the inverted soil profiles are shown in Figs. 59(a) and 60(a) in a solid line, which are compatible with the observed data. Figs. 59(b) and 60(b) show the V_s profiles estimated from the inversion.

The records during the earthquake of October 10, 1988, are used for this study. Since the epicenter of the 1988 event was located to the south of the city, only the E-W component motions are considered. The solid line in Fig. 61 shows the observed transfer function between the two sites $(A_{HG}/A_{JG})_{\text{obs}}$, in which A_{HG} and A_{JG} are the Fourier spectra of the ground accelerations at the two sites. The spectrum peak and minimum occurring 1.0–1.5 s and 0.3 s, appear to reflect the natural site periods at sites H and J, respectively.

Assuming that the layers at a depth of 90 m of site J and at a depth of 300 m of site H are the common bedrock, the ground surface amplifications relative

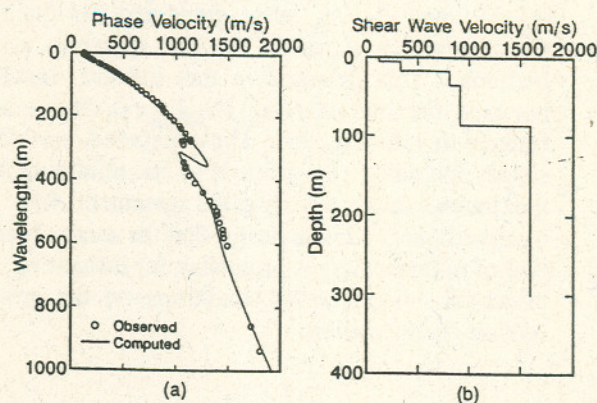


Fig. 59 Observed and computed dispersion curves and inferred V_s profile at site J⁵⁾

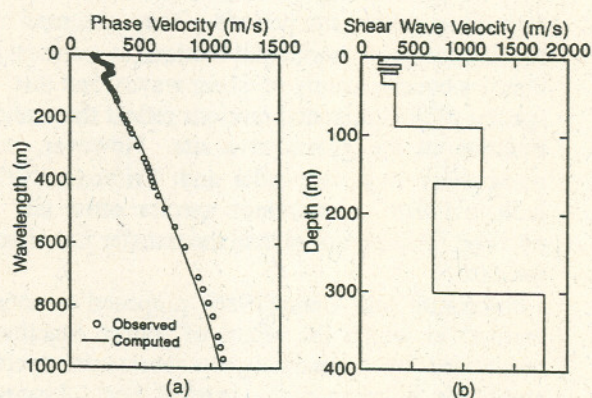


Fig. 60 Observed and computed dispersion curves and inferred V_s profile at site H⁵⁾

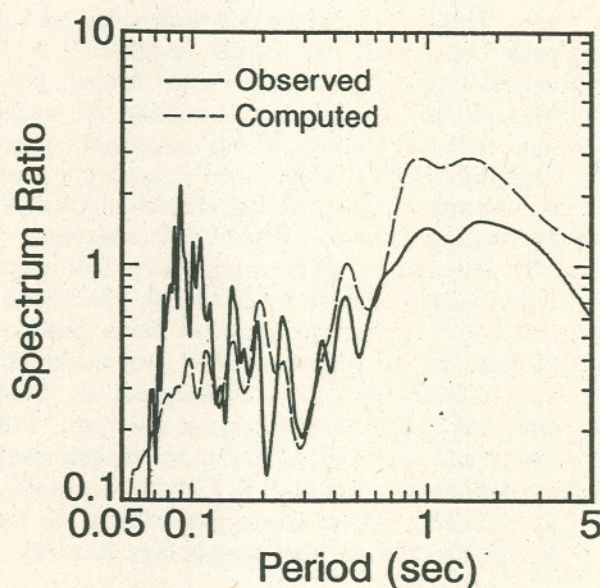


Fig. 61 Observed and computed spectrum ratio⁵⁾

to the bedrock of vertically propagating S-wave, A_{HG}/A_B and A_{JG}/A_B , were computed for the two sites, in which A_B is the Fourier spectrum at the bedrock. This resulted in the transfer function between the two sites $(A_{HG}/A_{JG})_{cmp}$, as shown in a broken line in Fig. 61. The computed spectrum shape, including the periods of its minimum and maximum, shows a fairly good agreement with the observed ones. This indicates that the array observation of microtremors is promising for estimating the effect of subsurface soil conditions on the ground motion characteristics.

MICROTREMOR SPECTRAL RATIOS

After the pioneer work by Kanai and Tanaka (1961), microtremor measurements at one station have been used for determining dynamic characteristics of sites as well as natural site periods. They assumed that the microtremor horizontal motions at periods less than 1 s consist mainly of shear waves, and that the spectra of the horizontal motions reflect the transfer function of the ground at a site. However, many researchers, e.g., Udawadia and Trifunac (1978), indicated that microtremor spectra often tell the exciting function rather than the transfer function of the site.

Nakamura and Ueno (1986) proposed a revised method in which the effect of source function is minimized by normalizing the horizontal spectral amplitude in terms of the vertical one. Assuming that the S-waves dominate in microtremors, they indicated that the horizontal-to-vertical (H/V) ratio of microtremors at a site roughly equals the S-wave transfer function between surface and bedrock at the site. This means that the H/V peak period and the peak value itself respectively correspond to the natural site period and the amplification factor. This method has the potential to make site periods more reliable; however, it rests on tenuous assumptions (Finn, 1991). In fact, the F-k spectrum analysis described in the preceding chapter indicates that microtremors consist mainly of surface waves.

To investigate what the microtremor H/V spectra reflect and whether the Nakamura's conclusion is reasonable, many studies have been conducted (Tokimatsu and Miyadera, 1992; Lermo and Chavez-Gracia, 1993, 1994; Tokimatsu et al., 1994a; Ohmachi et al., 1994; Wakamatsu and Yasui, 1995; Lachet and Bard, 1995). To summarize their results, the H/V spectra at sites A, B, J, and H described in the preceding chapter were computed from the following equation and are shown in Figs. 62 to 65.

$$H/V = \sqrt{S_{NS} S_{EW}} / S_{UD} \quad (63)$$

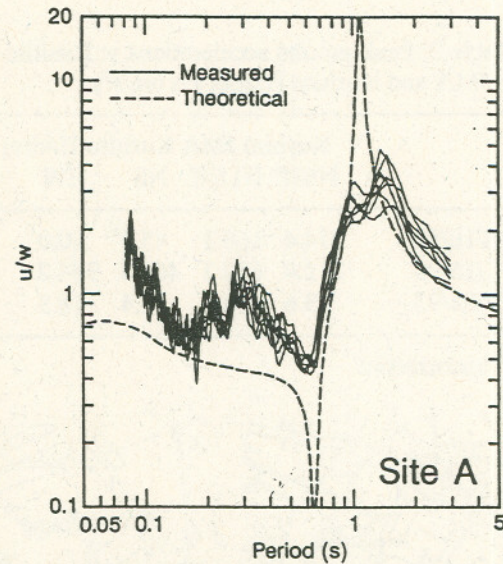


Fig. 62 H/V spectrum of microtremors compared with that of theoretical Rayleigh waves at site A (after Tokimatsu and Miyadera, 1992)⁶⁾

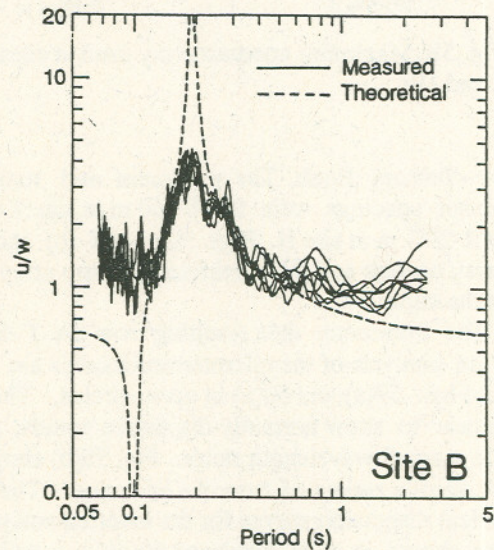


Fig. 63 H/V spectrum of microtremors compared with that of theoretical Rayleigh waves at site B⁶⁾

in which S_{UD} is the Fourier amplitude of microtremor vertical motions. Figs. 62 and 63 show all H/V spectra observed every 3 hours at sites A and B. As pointed out by Nakamura and Ueno (1986), the H/V spectra are stationary over a day and less affected by the source function of the site. The periods of the H/V peak at the four sites are 0.2, 1.37, 0.23, and 1.28 s, respectively. These values are in fairly good agreement with, but often slightly shorter than, the fundamental natural site periods of shear waves computed for the soil profiles shown in Figs. 30, 59, and 60, i.e., 0.21, 1.39, 0.29, and 1.57 s.

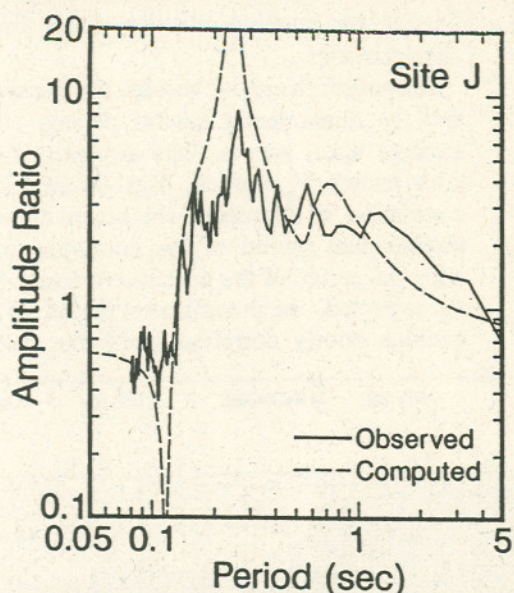


Fig. 64 H/V spectrum of microtremors compared with that of theoretical Rayleigh waves at site J (after Tokimatsu and Arai, 1995)⁷⁾

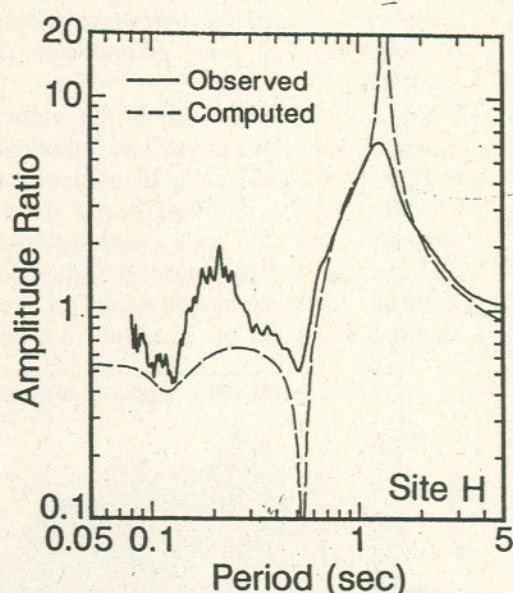


Fig. 65 H/V spectrum of microtremors compared with that of theoretical Rayleigh waves at site H⁵⁾

Also shown in Figs. 62 to 65 are the amplitude ratio (u/v) of the fundamental Rayleigh mode computed for the same profiles. The microtremor H/V spectra and their peak periods show good agreement with those of Rayleigh waves. This suggests that microtremors consist of predominant surface waves, and their H/V spectrum reflects that of Rayleigh waves (Tokimatsu and Miyadera, 1992).

The H/V value is, however, consistently larger than the Rayleigh-wave amplitude ratio except near the natural period. This is probably because the inclusion of Love waves and/or higher-mode Rayleigh waves in microtremor horizontal motions makes the H/V value defined by Eq. (62) larger than would be the case with Rayleigh waves only. By contrast, the H/V value near the natural site period is consistently smaller than the Rayleigh-wave amplitude ratio. This is probably because the inclusion of high-mode Rayleigh waves or body waves in microtremor vertical motions makes the H/V value defined by Eq. (62) smaller than would be the case with the fundamental Rayleigh mode only.

To draw a definite conclusion, Tokimatsu et al. (1994a) conducted microtremor measurements at 78 sites along a line crossing the Tokyo Bay area, as shown in Fig. 66. Fig. 67 shows the shear wave velocity logs available for 12 sites, and Fig. 68(a) shows the geologic cross section along the observation line. Figs. 67 and 68(a) indicate that a signifi-

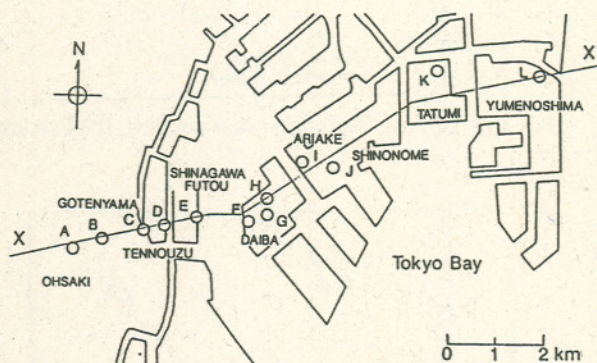


Fig. 66 Map showing location of test sites (after Tokimatsu et al., 1994a)⁷⁾

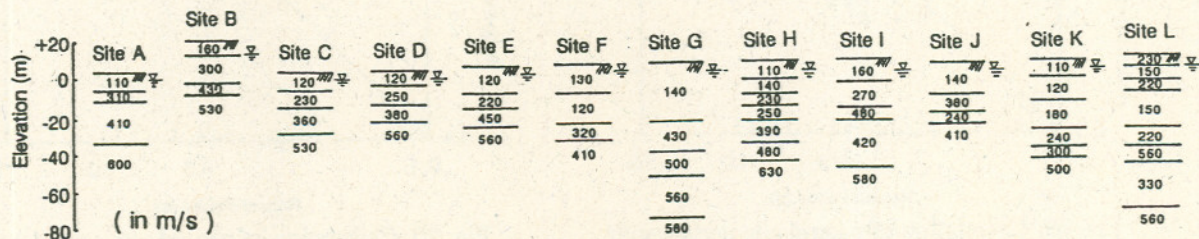


Fig. 67 Shear wave velocity logs at 12 sites⁷⁾

cant contrast exists in shear wave velocity between the alluvium (Holocene) and diluvium (Pleistocene) deposits.

Figs. 68 (b) and (c) show the variations of the predominant period of horizontal motions and of the period of H/V peak along the observation line. The variation of the H/V peak period does reflect the geologic profile in such a way that the larger the H/V peak period, the thicker the alluvial deposit. By contrast, the predominant period of the horizontal motions often occurs at about 0.3 s, probably re-

flecting the exciting function rather than the site characteristics.

To confirm the above results, the transfer function and the fundamental natural periods of vertically incident shear waves were computed for the sites with known V_s profiles. Figs. 69 and 70 show the correlation of the natural site period either with the predominant period of the horizontal motions or with the period of the peak microtremor H/V value. As expected, the predominant period of horizontal motions poorly correlates with the natural site

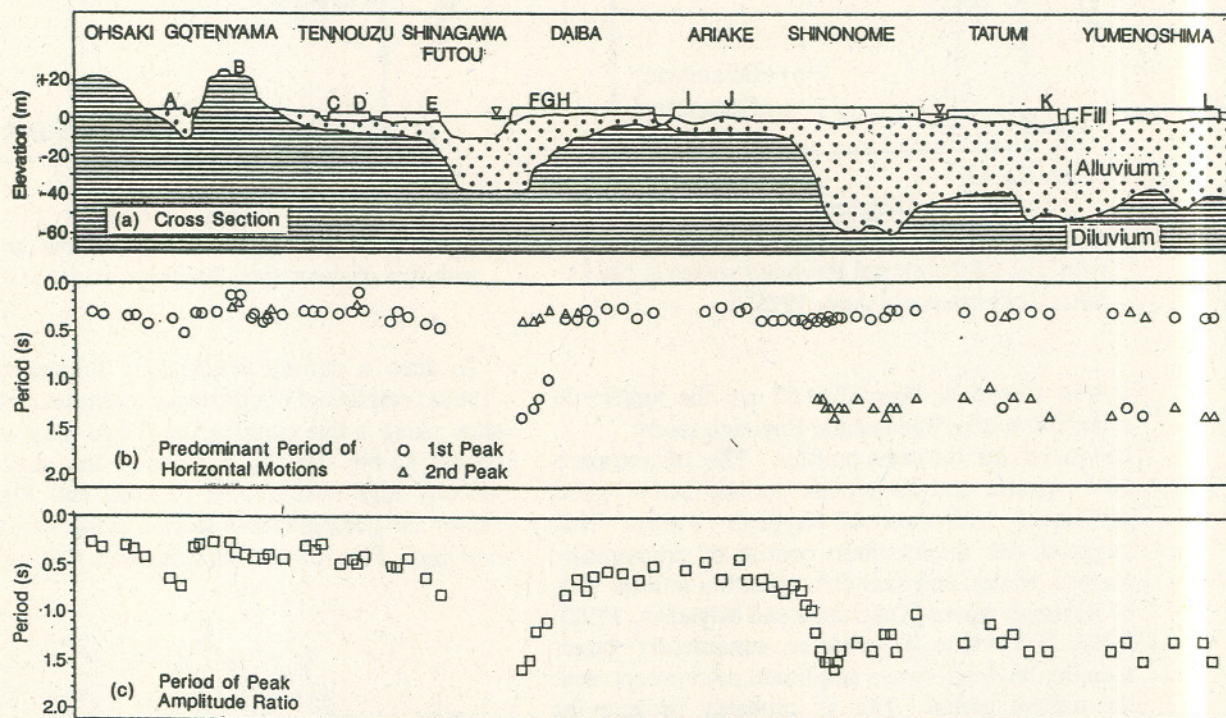


Fig. 68 (a) Geologic cross section, (b) Predominant period, and (c) Period of H/V peak⁷⁾

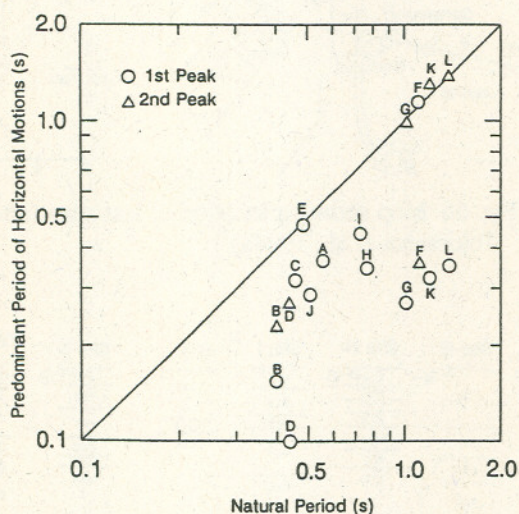


Fig. 69 Correlation of natural site period with predominant period of horizontal motions⁷⁾

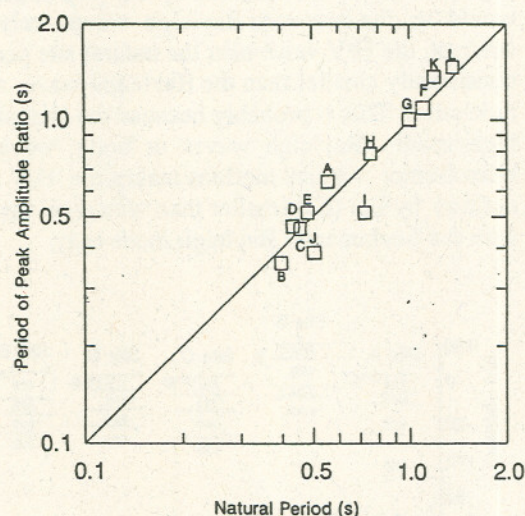


Fig. 70 Correlation of natural site period with period of microtremor H/V peak⁷⁾

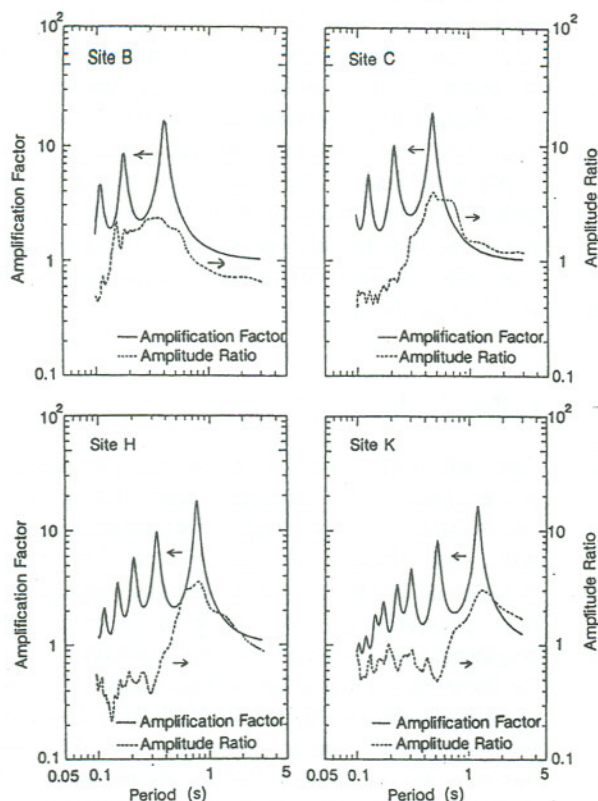


Fig. 71 Microtremor H/V spectra compared with transfer functions for four sites⁷⁾

period. The H/V peak period, by contrast, agrees fairly well with the natural site period. There are, however, some cases, e.g., sites I and J, in which the H/V peak period is slightly less than the natural site period. These sites appear to have lower impedance ratios between surface layer and bedrock. Such a trend affected by the impedance of the deposit is very analogous to that of Rayleigh wave amplitude ratio in two-layered media described previously.

Fig. 71 compares the microtremor H/V spectra with the transfer function computed for four sites. Nakamura and Ueno (1986) indicated that the microtremor H/V spectra correspond to the transfer function of the site. However, these two are poorly correlated except for the agreement in the period of their peak values.

Fig. 72 compares the microtremor H/V spectra with the Rayleigh wave amplitude ratios at the four sites in which site B has the lowest impedance ratio. At sites C, H, and K with high impedance ratios, the Rayleigh wave amplitude ratios become infinite near the natural period and become zero near a half the natural period. At site B with the lowest impedance ratio, however, the Rayleigh wave amplitude ratio becomes neither infinite nor zero. These trends are in good agreement with the microtremor H/V spectra, and are consistent with the Rayleigh wave

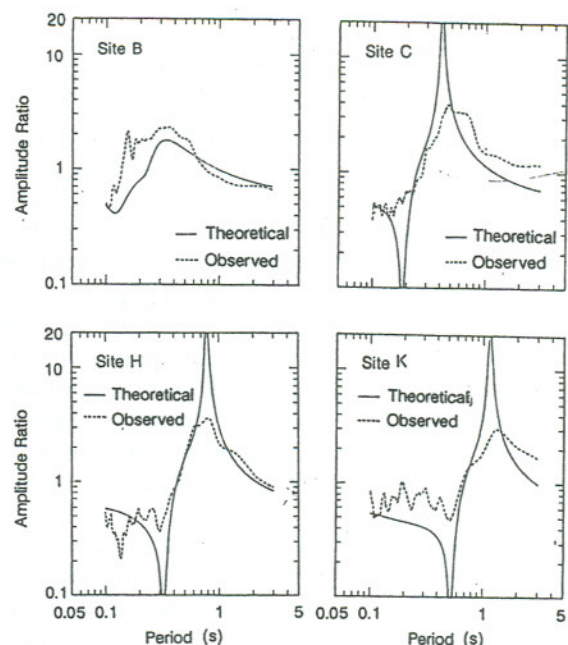


Fig. 72 H/V spectra of microtremors compared with those of Rayleigh waves⁷⁾

amplitude ratio of two-layered media with low impedance ratios.

Tokimatsu et al. (1994b) conducted microtremor measurements at over 10 strong motion downhole array stations where the transfer functions for the sites during earthquakes are available. The observed microtremor H/V peak values were then compared with the maximum amplification factor between surface and bedrock in terms of Fourier spectra. Fig. 73 summarizes the results for 10 sites with re-

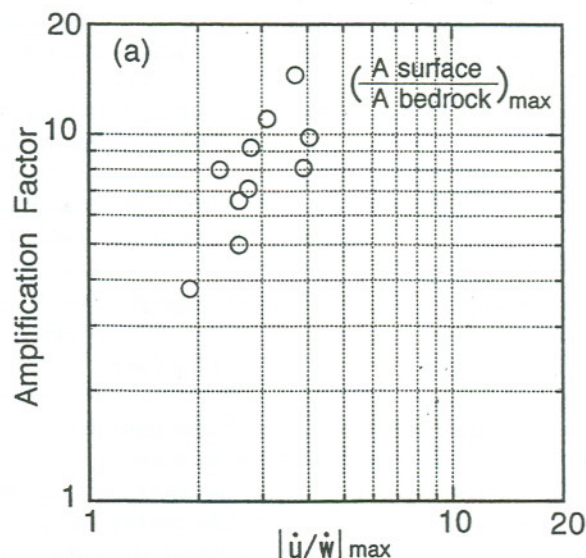


Fig. 73 Microtremor H/V peaks compared with amplification factors (Tokimatsu et al., 1994b)

latively high impedance ratios. Although the relation may not be necessarily 1 to 1, there is a trend in which the higher the H/V value the higher the amplification factor becomes. Based on the analyses of strong motion records and microtremor data, Lermo and Chavenz-Gracia (1993, 1994) and Wakamatsu and Yasui (1995) showed similar results.

The writer, however, believes that the above trend merely reflects the fact that both the amplification factor and the Rayleigh wave peak amplitude ratio tend to increase with increasing impedance ratio of the site. In addition, the F-k analysis of microtremors has shown that the microtremor H/V spectra reflect mainly the Rayleigh wave amplitude ratios and do not correspond the vertically-incident shear wave transfer function directly. Based on numerical studies, Lachet and Bard (1995) drew similar conclusions.

Finally, the above discussions indicate that if the microtremor H/V spectrum of a site has a distinct peak and a distinct minimum, the impedance ratio of the site is moderate to high. The natural period of the site could be equal to or 10-20 percentage points larger than the period of the H/V peak; or approximately equal to twice the period of the H/V minimum. The natural period thus estimated, however, may not always correspond to the fundamental site

period, but may reflect the second one or the depth of the interface between layers with the high impedance ratio. In addition, if the microtremor H/V spectrum of a site has neither distinct maximum nor minimum, the impedance ratio of the site is low, e.g., soil site with V_s gradually increasing with depth or rock site. The natural site period of the site cannot be determined from microtremor measurements made with only one station. Table 4 summarizes site characterization methods using microtremors so far discussed.

CONCLUDING REMARKS

The field techniques and analytical procedures for geotechnical site characterization using surface waves have been reviewed and summarized together with their theoretical background. A modified version of the wavenumber integral approach has been presented for calculating the ground surface displacements induced by a point source acting on the three-dimensional layered medium. The effects of body waves and higher-mode Rayleigh waves on the dispersion curves observed by the SASW method, were studied using three four-layered models. The results have shown the following:

(1) In most of layered media, the effects of body waves on the dispersion curve can be neglected, if the distance from the source exceeds a quarter of the wavelength measured.

(2) When a stiff layer overlies a soft layer, body waves may have significant effects on the observed dispersion curve. The affected wavelength ranges up to about twice the thickness of the stiff surface layer.

(3) The one dimensional F-k spectrum analysis method using more than two sensors could yield a dispersion curve more close to that of Rayleigh waves, even if observed waves are contaminated by body waves.

(4) For deposits with V_s increasing with depth, the fundamental Rayleigh-mode generally dominates, though a higher mode or multiple modes exist to some extent. For deposits with V_s varying with depth, on the other hand, a higher-mode or multiple modes dominate in some frequency range.

The F-k spectrum analysis and auto-correlation analysis for microtremor three-component motions have been introduced, and phase velocity dispersion characteristics of microtremors have been investigated. The main conclusions derived from the study are:

(1) The F-k spectrum analysis of the microtremor vertical components can provide dispersion characteristics of Rayleigh waves that are stationary over

Table 4 Classification of Site Characterization Methods Using Microtremors

Method	Number of Observation Points	Component Motions of Interest	Waves Assumed	Major Result
Spectrum Method	1	Horizontal	Shear Waves	Predominant Period ^{*1}
	1	Horizontal /Vertical	Rayleigh Waves	Natural Site Period ^{*2}
Phase Velocity Method	Many	Vertical	Rayleigh Waves	Shear Wave Profile
	Many	Horizontal	Rayleigh & Love Waves	Shear Wave Profile

^{*1} may not reflect the response characteristics of the site but the exciting function of the source.

^{*2} may not be identified if the impedance ratio of the deposit is low and may reflect the depth of the interface between layers with highest impedance ratio in the deposit and thus may not correspond to the fundamental natural period.

periods of a day, even if the source effects have a significant effect on microtremor ground motions.

(2) The F-k spectrum analysis on microtremor horizontal motions appears capable of extracting one of the dominant surface waves, i.e., generally Love waves, even through microtremors propagate from various directions. If microtremors propagate from one direction, both Rayleigh and Love characteristics may be obtained.

(3) The response factor, the medium response divided by the wavenumber of the square root of wavenumber, is an efficient indicator to determine the prevailing mode of surface waves in dispersion data.

(4) The F-k spectrum analysis and the auto-correlation analysis of microtremor vertical motions can yield almost the same dispersion curves, on the condition that the observed microtremors can be considered as unidirectional or isotropic waves; otherwise, the auto-correlation analysis may result in lower phase velocities.

Based on the above findings, the methods for constructing simulated dispersion curves have been presented both for the active SASW method and the frequency-wavenumber analysis of microtremors method, and the following suggestions and conclusions may be made.

(1) If the observed data are inversely dispersive, the effects of multiple modes should be taken into account in the inverse analysis.

(2) Use of either the dispersion data of the horizontal motion or the amplitude ratio of particle motions, in addition to the dispersion data of the vertical motion, may reduce the nonuniqueness of the soil profiles resulting from the inverse analysis.

Use of both Rayleigh wave phase and group velocities or both Rayleigh and Love wave phase velocities may also be suggested.

(3) The S-wave structures estimated from microtremor data, show good agreement with those obtained by the down-hole method to a depth approximately equal to the maximum array diameter used.

The frequency-wavenumber analysis of microtremors method may provide shear structures that are less sensitive and accurate than those from the down-hole method; nevertheless, it is appealing in that the test can readily be made at any time and at any place, by simply measuring microtremor ground motions with array of sensors. Besides, the advance of personal computers could make the field observation and data processing more reliable, much faster, and more cost effective. Thus, the method would be particularly useful for characterizing variation of soil conditions within a large area in a quick and economical manner. When using arrays with large apertures, this method can readily explore

down to the bedrock at deep soil sites. In those respects, it shows great promise particularly for preliminary site investigation, land use planning, and microzonation purposes.

Based on the F-k spectrum analysis, it seems reasonable to consider that the microtremor H/V spectra reflect mainly Rayleigh wave amplitude ratio and do not correspond the vertically-incident shear wave transfer function directly. For the estimation of the natural site period, the following guideline may be tentatively given:

(1) If the microtremor H/V spectrum of a site has a distinct peak and a distinct minimum, the impedance ratio of the site is relatively high. The natural period of the site could be equal to or 10-20 percentage points larger than the period of the H/V peak; or equal to twice the period of the H/V minimum.

(2) If the microtremor H/V spectrum of a site has neither distinct maximum nor minimum, the impedance ratio of the site is low, e.g., soil site having V_s gradually increases with depth or rock site. The natural site period of the site may not be determined from microtremor measurements at one station.

The natural period estimated from the above may not always correspond to the fundamental site period, but reflect the second one or the depth of the boundary between layers with the high impedance ratio. Thus, this method should be used in conjunction with other site investigation or with available geological or geophysical information. The use of H/V spectra supplemented by array observation of microtremors may be a preferable option for microzonation purposes.

ACKNOWLEDGMENTS

The author is grateful to Messrs. S. Tamura, H. Arai, and S. Mihara, Tokyo Institute of Technology, for their valuable assistance in the preparation of this paper.

REFERENCES

- Aki, K. (1957). "Space and time spectra of stationary stochastic waves, with special reference to microtremors," *Bulletin, Earthq. Res. Inst.*, 35, 415-456.
- Asten, M. W., and Henstridge, J. D. (1984). "Array estimator and the use of microseisms for reconnaissance of sedimentary basins," *Geophysics*, 49(11), 1828-1837.
- Barker, T. G. and Stevens (1991) "Array processing of Rayleigh waves for shear structure," *Proceedings, 2nd International Conference on Recent*

- Advances in Geotechnical Earthquake Engineering and Soil Dynamics, 2, 1393-1397.
- Capon, J. (1969). "High-resolution frequency-wavenumber spectrum analysis," *Proceedings, IEEE*, 57(8), 1408-1418.
- Dorman, J. and Ewing, M. (1962) "Numerical inversion of seismic surface wave dispersion data and crust-mantle structure in the New York-Pennsylvania area," *Journal of Geophysical Research*, Vol. 67, No. 13, pp. 5227-5241.
- Ewing, W. M., Jardetzky, W. S., and Press, F. (1957) "Elastic waves in layered media," McGraw-Hill.
- Finn, W. D. L. (1991). "Geotechnical engineering aspects of microzonation," *Proceedings, 4th Int. Conf. on Seismic Zonation*, Vol. 1, 199-259.
- Gabriels, P., Snieder, R., and Nolet, G. (1987). "In situ measurements of shear-wave velocity in sediments with higher-mode Rayleigh waves," *Geophysical Prospecting*, 35, 187-196.
- Gucunski, N., and Woods, R. D. (1991). "Use of Rayleigh modes in interpretation of SASW test," *Proceedings, 2nd International Conference on Recent Advances in Geotechnical Earthquake Engineering and Soil Dynamics*, 2, 1399-1408.
- Harkrider, D. G. (1964). "Surface waves in multilayered elastic media I. Rayleigh and Love waves from buried sources in a multilayered elastic half-space," *Bulletin, Seismological Society of America*, 54(2), 627-679.
- Haskell, N. A. (1953). "The dispersion of surface waves on multilayered media," *Bulletin, Seismological Society of America*, 43(1), 17-34.
- Haubrich, R. A. and McCamy, K. (1969) "Microseisms: coastal and pelagic sources, Review of Geophysics, Vol. 7, No. 3, pp. 539-571.
- Heukelom, W. and Foster, C. R. (1960) "Dynamic testing of pavements," *Journal of the Structural Division, ASCE*, SM1, pp. 1-28.
- Horiike, M. (1981) "Estimation of phase velocity of microtremors," *Zishin (Journal of Seismological Society of Japan)*, Ser 2, Vol. 34, pp. 535-550.
- Horiike, M. (1985) "Inversion of phase velocity of long-period microtremors to the S-wave-velocity structure down to the basement in urbanized area," *J. Phys. Earth.*, 33, 59-96.
- Iai, S., Matsunaga, Y., Morita, T., and Sakurai, H. (1994) "Performance of quay walls during the 1993 Kushiro-oki earthquake," *Proceedings, The 13th International Conference on Soil Mechanics and Foundation Engineering*, pp. 69-74.
- Jeffreys, H. (1962) "Small correction in the theory of surface waves," *Geophysical Journal of the Royal Astronomical Society*, 6, pp. 115-117.
- Jones, R. B. (1958) "In-situ measurement of the dynamic properties of soil by vibration methods," *Geotechnique*, Vol. 8, No. 1, pp. 1-21.
- Kanai, K., and Tanaka, T. (1961). "On microtremors. VIII," *Bulletin, Earthq. Res. Inst.*, 39, 97-114.
- Kashima, T. (1993) "Characteristics of strong earthquake motion observed at Kushiro local meteorological observatory," *Proceedings, The 21st Symposium of Earthquake Ground Motion*, pp. 27-32, (in Japanese).
- Lacoss, R. T., Kelly, E. J., and Toksöz, M. N. (1969). "Estimation of seismic noise structure using arrays," *Geophysics*, 34(1), 21-28.
- Lamb, H. (1904) "On the propagation of tremors over the surface of an elastic solid," *Phil. Trans. Soc. London*, Vol. 203, Series A, pp. 1-42.
- Lachet, C. and Bard, P. Y. (1995) "Theoretical investigations on the Nakamura's technique," *Proceedings, 3rd International Conference on Recent Advances in Geotechnical Earthquake Engineering and Soil Dynamics*, 2, pp. 671-675.
- Lermo, J. and Chavenz-Garcia, F. J. (1993) "Site effect evaluation using spectral ratios with only one station," *Bulletin of Seismological Society of America*, 83, 1574-1594.
- Lermo, J. and Chavenz-Garcia, F. J. (1994) "Are microtremors useful in site response evaluation?," *Bulletin of Seismological Society of America*, 84(5), 1350-1364.
- Liaw, A. L., and McEvilly, T. V. (1979). "Microseisms in geothermal exploration - studies in Grass Valley, Nevada," *Geophysics*, 44(6), 1097-1115.
- Matsushima, K. and Okada, H. (1990) "An exploration method using microtremors (2) - An experiment to identify Love waves in long-period microtremors -," *Proc., 82th Annual Meeting of SEGJ*, pp. 5-8 (in Japanese).
- Miller, G. F. and Pursey, H. (1955) "On the partition of energy between elastic waves in a semi-infinite solid," *Proceedings, Royal Society, London, Series A*, Vol. 233, pp. 55-69.
- Nakamura, Y. and Ueno, M. (1986) "A simple estimation method of dynamic characteristics of subsoil," *Proceedings, The 7th Japan Earthquake Engineering Symposium*, pp. 265-270, (in Japanese).
- Nazarian, S., and Stokoe, K. H., II (1984). "In situ shear wave velocity from spectral analysis of surface waves," *Proceedings, 8th World Conference on Earthquake Engineering*, 3, 31-38.
- Nazarian, S., and Stokoe, K. H., II (1986). "Use of surface waves in pavement evaluation," *Transportation Research Record*, 1070, 132-144.
- Nazarian, S. and Desai, M. R. (1993) "Automated surface wave method: Field testing," *Journal of Geotechnical Engineering, ASCE*, Vol. 119, No.

- 7, pp. 1094-1111.
- Ohmachi, T., Konno, K., Endoh, T., and Toshinawa, T. (1994) "Refinement and application of an estimation procedure for site natural periods using microtremor," *Journal of JSCE*, No. 489, I-27, pp. 251-260 (in Japanese).
- Okada, H. and Matsushima, T. (1986). "Estimation of under-ground structures down to a depth more than several hundreds of meters using long-period microtremors," *Proceedings, 7th Japan Earthquake Engineering Symposium*, 211-216 (in Japanese).
- Saito, M. (1993) "Branch line contribution in Lamb's problem," *Butsuri-Tansa*, Vol. 46, No. 5, pp. 372-380 (in Japanese).
- Saito, M. and Kabasawa, H. (1993) "Computations of reflectivity and surface wave dispersion curves for layered media II. Rayleigh wave calculations," *Butsuri-Tansa*, Vol. 46, No. 4, pp. 283-298 (in Japanese).
- Sanchez-Salinerio, I., Roësset, J. M., Shao, K.-Y., Stokoe, K. H. II, and Rix, G. J. (1987) "Analytical evaluation of variables affecting surface wave testing of pavements," *Transportation Research Record* 1136, pp. 86-95.
- Sheu, J. C., Stokoe, K. H. II, and Roësset, J. M. (1989) "Effect of reflected waves on SASW testing of pavements," *Transportation Research Record* 1196, pp. 51-61.
- Stokoe, K. H., II, and Nazarian, S. (1985). "Use of Rayleigh waves in liquefaction studies," *Proceedings, Measurement and Use of Shear Wave Velocity for Evaluating Dynamic Soil Properties*, Geotechnical Engineering Division, ASCE, 1-17.
- Stokoe, K. H., II, Nazarian, S., Rix, G. J., Sanchez-Salinerio, I., Sheu, J. C., and Mok, Y. J. (1988). "In situ seismic testing of hard-to-sample soils by surface wave method," *Earthquake Engineering and Soil Dynamics II - Recent Advances in Ground Motion Evaluation*, Geotechnical Special Publication No. 20, ASCE, pp. 264-278.
- Takeuchi, H. and Saito, M. (1972) "Seismic surface waves", *Methods in Computational Physics*, Vol. 11, Academic Press, pp. 217-295.
- Thomson, W. T. (1950). "Transmission of elastic waves through a stratified soil medium," *Journal of Applied Physics*, 21, 89-93.
- Tokimatsu, K., Kuwayama, S., Tamura, S., and Miyadera, Y. (1991). " V_s determination from steady state Rayleigh wave method," *Soils and Foundations*, 31(2), 153-163.
- Tokimatsu, K. and Miyadera, Y. (1992) "Characteristics of Rayleigh waves in microtremors and their relation to shear structures," *Journal of Structure and Construction Engineering*, AIJ, No. 439, pp. 81-87 (in Japanese).
- Tokimatsu, K., Tamura, S., and Kojima, H. (1992a) "Effects of multiple modes on Rayleigh wave dispersion," *Journal of Geotechnical Engineering*, ASCE, 118(10), 1529-1543.
- Tokimatsu, K., Shinzawa, K., and Kuwayama, S. (1992b). "Use of short-period microtremors for V_s profiling," *Journal of Geotechnical Engineering*, ASCE, 118(10), 1544-1558.
- Tokimatsu, K., Miyadera, Y., and Kuwayama, S. (1992c) "Determination of shear wave velocity structures from spectrum analyses of short-period microtremors," *Proc., 10th World Conference on Earthquake Engineering*, Vol. 3, pp. 253-258.
- Tokimatsu, K., Nakajo, Y., and Tamura, S. (1994a) "Horizontal-to-vertical amplitude ratio of short period microtremors and its relation to site characteristics," *Journal of Structure and Construction Engineering*, AIJ, No. 457, pp. 11-18 (in Japanese).
- Tokimatsu, K., Hijikata, K., Nakajo, Y., and Tamura, S. (1994b) "Amplification of subsurface soils estimated from microtremor measurements," *Proc., Annual Meeting of JSSMFE*, pp. 1133-1134 (in Japanese).
- Tokimatsu, K. and Arai, H. (1995) "Estimation of local site conditions in Kushiro city based on array observation of microtremors," *Proceedings, 3rd International Conference on Recent Advances in Geotechnical Earthquake Engineering and Soil Dynamics*, 2, pp. 599-602.
- Tokimatsu, K., Arai, H., and Sakai, J. (1995) "Characteristics of surface waves in short-period microtremors and their relation to shear structures," *Journal of Structure and Construction Engineering*, AIJ, No. 472, pp. 47-55 (in Japanese).
- Tokimatsu, K. and Tamura, S. (1995) "Contribution of Rayleigh and body waves to displacement induced by a vertical point force on a layered elastic half-space," *Journal of Structure and Construction Engineering*, AIJ, No. 476, pp. 95-101 (in Japanese).
- Toksöz, M. N. (1964). "Microseisms and an attempted application to exploration," *Geophysics*, 29(2), 154-177.
- Udwadia, F. E. and Trifunac, M. D. (1973). "Comparison of earthquake and microtremor ground motions in El Centro, California," *Bulletin, Seismological Society of America*, 63(4), 1227-1253.
- Wakamatsu, K. and Yasui, Y. (1995) "Possibility of estimation for amplification characteristics of soil deposits based on ratio of horizontal to vertical spectra of microtremors," *Journal of Structure and Construction Engineering*, AIJ, No. 471, pp. 61-70.

- Wiggins, R. A. (1972) "The general liner inversion problem: Implication of surface waves and free oscillations for earth structure," *Reviews of Geophysics and Space Physics*, Vol. 10, No. 1, pp. 251-285.
- Woods, R. D. (1968) " Screening of surface waves in soils," *Journal of the Soil Mechanics and Foundations Division, ASCE*, Vol. 94. No. SM4, pp. 951-979.
- Yuan, D. and Nazarian, S. (1993) "Automated surface wave method: Inversion Technique," *Journal of Geotechnical Engineering, ASCE*, Vol. 119, No. 7, pp. 1112-1126.